Accuracy of Surface-Potential-Based Long-Wide-Channel MOS Transistor Compact Models

Bin B. Jie and Chih-Tang Sah

University of Florida
Gainesville, Florida 32611-6200
Emails: binjie@UFL.edu, tctsah@UFL.edu

ABSTRACT

This paper answers the frequently asked question, "How accurate are the approximate baseline long-and-wide-channel MOS transistor models that have been used to develop the compact models for computer-aided circuit designs?" Three commonly used surface-potential-based ($U_S=q\psi_S/kT$) approximations of the bulk-charge are evaluated: $Q_B \propto$ (i) $(U_S)^{1/2}$, (ii) $(U_S-1)^{1/2}$, and (iii) $[U_S-1+\exp(-U_S)]^{1/2}$. Self-consistent remote charge neutrality boundary condition, minority carriers, and space constant impurity concentration and oxide thickness are used. Percentage deviations of the approximations from the non-compact baseline model are computed for DC drain current, drain- and trans-conductances. Approximation (i) shows significant devia-tions, ~16% at threshold diverging rapidly with deepening into the subthreshold range. Approximations (ii) and (iii) show a few percent (1% to 2%) deviations in both inversion and subthreshold ranges, but diverge widely below sub-threshold and in accumulation. A new analytical model is tested and shows better than 10% accuracy in accumulation.

Keywords: MOSFET, MOST, bulk charge approximations, baseline model, four-component space-charge theory, surface potential model, self-consistent remote charge boundary condition.

1 INTRODUCTION

The existing compact models of Metal-Oxide-Silicon field-effect Transistor (MOSFET or MOST) can be sorted into three groups [1,2,3]: the threshold-voltage [4,5], inversion-charge [5,6], and surface-potential [6] models, the latter two succinctly compared in [3]. All are analytical approximations to the 4-terminal (Gate, Drain, Source, Basewell or Body) electrical characteristics of the 2-dimensional (2-D) transistor. In the initial approximations starting with a long-wide baseline geometry, the 2-D transistor is partitioned into a 1-D MOS capacitance (MOSC) governed by the x-equation which gives the input gate-voltage equation, $V_G(U_S)$, and a 1-D variable resistance (MOSR) or transistor (MOST) governed by the y-equation which gives the output drain-current equation, $I_D(U_S)$. The surface potential, $U_S=q\psi_S/kT$, is the independent variable. It is the total variation or total bending of the one-electron energy-band in the x-direction from the SiO_2/Si interface (x=0) to the remote boundary ($x=\infty$). It couples these two 1-D equations, $V_G(U_S)$ and $I_D(U_S)$, to give the output drain current as a function of the input gate voltage, or the transfer characteristics, $I_D(V_G)$, and the output drain current as a function of the output drain voltage, or the output characteristics, $I_D(V_D)$. The source and basewell (or body) voltages, V_S and V_B, are used as the reference or parameter. In the last 25 years (since about 1980), compact-model-development engineers have been developing fast convergent algorithms to solve the implicit equation, $V_G(U_S)$, in order to give very accurate surface potential U_S (~ $<10^{-10}$ error near flatband, $U_S \rightarrow 0$), at a given V_G, over the entire V_G range from accumulation, through flatband and subthreshold, into inversion. Such accuracy is required for circuit design applications using computer-aided-design circuit simulators such as SPICE. This was circumvented in the threshold-voltage compact models by use of the linear approximation, $U_G \approx U_S$ to give $I_D[U_S(V_G)]=I_D[V_G(U_S)]=I_D(V_G)$. The Berkeley threshold-voltage model, BSIM [7], has been the industry standard for the last decade (1995-2005) because of computation speed and equation simplicity for user modifications, in spite of the many empirical approximations (in addition to the threshold voltage assumption) which it has used to represent the 2-D small-geometry effects, the spatially varying material parameters, and the large-deviation-from-thermal-equilibrium or hot-carrier effects. Linearization was also employed by the inversion charge model [3] to replace the surface potential by inversion-charge as the independent variable.

With the many-order increase of computer speed in recent years, revival of the intrinsically more accurate surface-potential-based model was proposed as the baseline model [8]. In May 2005 the international Compact Model Council selected two surface-potential-based compact models as the finalists for the next generation MOSFET compact-model standard [9], the PSP (Penn-State-University and Phillips) [10] and the HiSIM (Hiroshima University) [11] models. Recently, PSP was selected by a slim margin, 16 vs 14 votes.

Both HiSIM and PSP models employ the surface potential to analyze their long and wide channel baseline

MOS transistor. Both stated the use of the 1978-Brews charge-sheet approximation [12] for the y-equation (current-equation) by confining the minority carrier or inversion charge density to a thin x-layer at the SiO_2/Si interface, x=0, which was rigorously expressed by the Dirac delta-function δ(x) [1]. HiSIM fully implements the nonlinear implicit x- or voltage-equation $V_G(U_S)$. PSP makes a further simplification by linearization. The surface potential is then used as the independent variable to include, by analytical approximation, all the geometric, bias, and physical effects [2,10,11], such as short-channel, narrow-channel, bias- and geometry-dependences, longitudinal field gradient (The term 'lateral' field gradient has been used, but this is a misnomer, since x-dependence or lateral-dependence of the y-component electric field in the long-wide channel has not been taken into account in the 'charge-sheet' δ(x) approximation of the baseline model.), finite-thickness space-charge-layer in polycrystalline-silicon-gate known as gate-depletion, quantum-mechanical confinement in the silicon surface layer at the SiO_2/Si interface, thin-gate-oxide tunneling, pocket implants at the drain and source regions, bias dependent overlap capacitances, gate-induced drain leakage, noise, and others.

Several leading compact-model developers have recently indicated to us a strong interest on knowing the accuracy of the baseline (long-wide channel) surface-potential-based compact models which they have used, since their baseline models originated from our analyses in 1964, 1965 and 1966 [4,5,6]. In response, this paper gives an evaluation on the accuracy of the DC characteristics. RF characteristics will be reported in the future.

2 THEORETICAL FORMULAS

The two-dimensional (2-D) direct-current (DC) equations for a wide (z-direction) and long (y-direction) electron-channel (n-channel) MOS transistor are given by the Poisson Equation for the electric field and electric (electrostatic) potential and the two-mechanism current equation of the drift and diffusion mechanisms. With a basewell-channel impurity concentration of $P_{IM}(x,y)$, an electron drift mobility of $\mu_n(x,y)$ and an electron diffusivity of $D_n(x,y)$, in a semiconductor with dielectric constant $\varepsilon(x,y)=\varepsilon$, these two equations are given by

$$\varepsilon \nabla \mathbf{E}(x,y) = \rho(x,y) = q[P(x,y) - N(x,y) - P_{IM}(x,y)] \quad (1)$$

$$\mathbf{J}_N(x,y) = q\mu_n(x,y) N(x,y) \mathbf{E}(x,y) + qD_n(x,y) \nabla N(x,y) \quad (2)$$

The exact solutions can only be obtained numerically. To develop analytical compact models in order to give high accuracy in short computation times for extractions of device and materials parameters from experimental data, the following assumptions are made first to give the baseline model. Refinements of the baseline model are then made (beyond the objective of this paper, see references cited by [2] for the refinements) by analytical approximations to account for the realistic effects from 2-D small-geometry, spatial-varying materials properties, and deviation from thermodynamic equilibrium at high electric fields (from small-geometry). This paper provides theoretical accuracy of the analytical baseline compact models whose deviations come from assumptions made in their derivations from the exact integral equations. The assumptions are as follows. (i) The p-type basewell impurity concentration is spatially constant, $P_{IM}(x,y)=P_{IM}$, in the n-type inversion channel region. (ii) The channel is terminated by two highly-doped n-type regions, the n++Source and n++Drain, and the short-channel effects from the Drain and Source n++/p-basewell junction space-charge-regions are not taken into account. (iii) The electric field (in the x-direction), produced by the voltage applied between the gate and the basewell or body contacts, dominates over the electric field (in the y-direction), produced by the voltage applied between the drain and source, $|E_X(x,y)| >> |E_Y(x,y)|$. Based on these three assumptions, the 2-D Poisson Equation, (1), is then simplified to the 1-D Poisson Equation in the x-direction.

$$\varepsilon \partial E_X(x)/\partial x = \rho(x,y) = q[P(x,y) - N(x,y) - P_{IM}] \quad (3)$$

The current is assumed to be confined in the y-direction, valid for long channels. Then, the vector current equation, (2), reduces to the 1-D current equation in the y-direction. It is further simplified by assuming small deviation from thermal equilibrium or quasi-equilibrium as coined by Shockley, i.e. the electron kinetic temperature is negligibly higher than the lattice-vibration temperature, $T_e(x,y,z) = T(x,y,z)$, which is spatially constant or has negligible local thermal heating $T(x,y,z)=T$. It is further assumed that electron and hole concentrations are low, so that the Boltzmann approximation or exponential representation can be used, $N=n_i\exp(+U-U_N)$ and $P=n_i\exp(+U_P-U)$. The normalized electric potential is $U=q\psi/kT \equiv qV_I/kT$ and the normalized electrochemical or quasi-Fermi potentials (coined by Shockley) for electrons and holes are $U_N=qV_N/kT$ and $U_P=qV_P/kT$. Then the Einstein relationship holds, $D_n[P_{IM}(x,y),T_e(x,y)] \div \mu_n[P_{IM}(x,y),T_e(x,y)] = D_n(P_{IM},T) \div \mu_n(P_{IM},T) = kT/q$. These reduce y-component of the 2-D conduction current density, $J_{NY}(x,y)$, given by (2), to a simpler 1-D 2-term equation, and also a 1-D 1-term gradient equation of electrochemical potential, or quasi-Fermi potential, $\nabla V_N(x,y)$. Using the macroscopic electric field, $E_Y(x,y) \triangleq -\partial V(x,y)/\partial y = -(kT/q)\,\partial U(x,y)/\partial y$, these are:

$$J_{NY}(x) = +q\mu_n N(x,y) E_Y(x,y) + qD_n \partial N(x,y)/\partial y \quad (4)$$

$$= -q\mu_n N(x,y) \partial V_N(x,y)/\partial y \quad (5)$$

Using these assumptions and approximations, the 1-D Poisson Equation, (3), simplifies to

$$\partial^2 U/\partial X^2 = [\exp(+U_P - U) - \exp(+U - U_N) - (P_{IM}/n_i)] \quad (6)$$

where X is the x-distance normalized to the intrinsic Debye length, $X=x/L_{Di}$, and $L_{Di} = (\varepsilon kT/2q^2n_i)^{1/2}$. All the three potentials, U, U_P, and U_N, are functions of (x,y). The Boltzmann or exponential transformation of carrier concentrations and electrochemical or quasi-Fermi potentials used in (4) to give (5) are

$$N(x,y)=n_i\exp\{(q/kT)[+V(x,y)-V_N(x,y)]\}\equiv n_i\exp(+U-U_N) \quad (7)$$
$$P(x,y)=n_i\exp\{(q/kT)[+V_P(x,y)-V(x,y)]\}\equiv n_i\exp(+U_P-U) \quad (8)$$

If it is assumed that the electrochemical potentials or the quasi-Fermi potentials of electrons and holes are independent of x, $U_P(x,y)=U_P(y)$ and $U_N(x,y)=U_N(y)$, first given in 1965-Sah [5], then the Poisson Equation, (6), can be integrated along x at a given y, once by quadrature in dU and twice in dxdx. Then, the boundary conditions of the electric field and electric potential or applied voltage can be applied at the three interfaces, the gate-metal/oxide ($x=-X_{OX}$), oxide/Silicon (x=0) and Silicon/body-metal ($x=\infty$). The x-independence assumption of the quasi-Fermi potentials is consistent with the assumptions of the current is flowing only in the y direction and the y-component of the electric field is small compared with the x-component of the electric field in the semiconductor and also in the gate insulator. The combination of the two integration solutions (in dU and dxdx) gives the voltage-equation [1]:

$$U_{GB}-U_{FB}-U_S=U_{OX}=2U_{II}^{1/2}\times \mathrm{Sign}U_S\times F_{SI}(U_S,U_{P0},U_{P\infty},U_{N0},U_{N\infty}) \quad (9)$$

where the square of the normalized normal or x-component of the electric field is

$$F_{SI}^2=+[+\exp(-U_S)+(+U_S-1)\exp(-U_{P0}+U_{P\infty})]\exp(+U_{P0}) + [+\exp(+U_S)+(-U_S-1)\exp(+U_{N0}-U_{N\infty})]\exp(-U_{N0}) \quad (10)$$

Here, $U_{II}=(q/kT)(\varepsilon_S qn_i/2C_O^2)$ and $C_O=\varepsilon_O/x_O$. (U_{P0},U_{N0}) and $(U_{P\infty},U_{N\infty})$ are respectively the (hole, electron) quasi-Fermi potentials at interface (x=0) and at the remote boundary ($x=\infty$). In this inversion n-channel MOST example, the first three terms in (10), with multiplier $\exp(+U_{P0})$, are from majority carriers or holes in the p-basewell and the second three terms, with multiplier $\exp(-U_{N0})$, are from minority carriers or electrons. In the x-independent quasi-Fermi assumption used to obtain (9) and (10), we wrote $U_{P0}(y)\triangleq U_P(x=0,y)$, $U_{P\infty}(y)\triangleq U_P(x=\infty,y)$, $U_{N0}(y) \triangleq U_N(x=0,y)$ and $U_{N\infty}(y) \triangleq U_N(x=\infty,y)$. Three solutions of (10) were given by Sah in 2005-Sah [1]. {See Eqs.(21.25), (21.28) and (21.31) on pp. 359-361 of [1] where $\xi(y)\triangleq U_N(y)-U_P(y)$.} (i) The term $\exp(-U_{NP})$ or $\exp(-\xi)$ multiplies only <u>one</u> of three minority carrier (electron) terms in (10), $[\exp(+U_S)]$, using the assumptions $U_{N0}=U_N\neq U_F$, $U_{P0}=U_P\neq U_F$, and $U_{N\infty}=U_{P\infty}=U_F$. (ii) The term $\exp(-U_{NP})$ or $\exp(-\xi)$ multiplies only <u>two</u> of three minority carrier terms in (10), $[\exp(+U_S)-1]$. This was derived in 1964 and used in the 1965-Sah-Pao x-equation [5]. It was more rigorously re-derived by Sah in 2004 [1] assuming $U_{N0}=U_N\neq U_F$, and $U_{N\infty}=U_F=U_P=U_{P0}=U_{P\infty}$. This was used by all subsequent compact-model developers since its first use in 1965-Sah-Pao [5]. It has the imaginary x-component electric field trouble [1] near flatband and causes nonconvergence in the numerical iteration solution of U_S for a given U_{GB} near the flat band U_{FB}. (iii) This is the <u>Self-Consistent Remote Charge-Neutrality Solution</u> derived by Sah in 2004 [1] which takes into account of minority carriers at the remote boundary to give $U_{N\infty}=U_{N0}=U_N\neq U_F$ and $U_{P\infty}=U_{P0}=U_P\neq U_F$, rather than the incorrect relations $U_{N\infty}=U_{N0}=U_N=U_{NP}+U_F$ and $U_{P\infty}=U_{P0}=U_F$, then the term $\exp(-U_{NP})$ or $\exp(-\xi)$ multiplies all three minority carrier terms, $[\exp(+U_S)-U_S-1]$. This is used in this paper as the baseline solution. The inconsistent solutions (i) and (ii) are listed here for history but also because they correspond to solutions of finite recombination at the remote boundaries and in the p-bulk or p-basewell, although their solutions near flatband would still be incorrect.

However, (iii) gives a divergent drain current at flatband, when computed by integrating (5) across the transistor cross-sectional area, $\iint dxdz$, as $z\rightarrow\infty$, at any y. This is due to the assumptions of no-recombination-generation and x-independent electron and hole quasi-Fermi-potentials. This divergence of the drain current was not noticed in previous papers since the drain current near flatband is so small that it was neglected by all previous investigators. To remove this divergence, the equilibrium or flat-band minority carrier concentration at the remote boundary, N_∞, is subtracted from the total electron concentration, N, in (5). This gives the non-divergent or bounded current-equation which does not diverge at flatband.

$$I_D=-\int_z\int_y\int_x[J_{Ny}(x,y)-J_{NyFB}(x,y)]\,dx\,(dy/L)\,dz = (Z/L)\int_y\int_x q\mu_n[N(x,y)-N(x=\infty,y)][\partial V_N(x,y)/\partial y]\,dxdy \quad (11)$$

where z=0 to Z, y=0 to L or $U_N=U_N(y=0)=U_{N0}$ to $U_N(y=L)=U_{NL}$, and x=0 to ∞ or $U(x=0,y)=U_S(y)$ to $U(x=\infty,y)=0$. Equation (11) is the 1-term double integral current equation in 1966-Pao-Sah [6], with the flatband current subtracted here. Using the U's and assuming constant mobility, (11) reduces

$$I_D = \frac{Z}{L} qD_n n_i L_{Di} \int_{U_{N0}}^{U_{NL}} \exp(-U_N)\,dU_N \int_0^{U_S} \frac{[\exp(+U)-1]dU}{\mathrm{Sign}U_S\times F_X(U,U_N,U_P)} \quad (12)$$

where -1 in $[\exp(+U)-1]$, comes from the subtraction of the unbounded flatband current. The multiplier or normalization factor, $I_{NORM}=(Z/L)\times qD_n n_i L_{Di}$ is 5.55×10^{-11}A/(Z/L) or Ampere per square, (Z/L)=1, for the device parameters we are using in this paper, $P_{IM}=1\times10^{18}\mathrm{cm}^{-3}$, $X_{OX}=2.0$nm, $\mu_n=400\mathrm{cm}^2$/V-s, and $n_i=1.33\times10^{10}\mathrm{cm}^{-3}$ at T=300K. The following are used.

$$[F_X(U,U_N,U_P)]^2=[\exp(-U)+U-1]\exp(+U_P) + [\exp(+U)-U-1]\exp(-U_N) \quad (13)$$
$$P_\infty/n_i=\exp(+U_P)=[(P_{IM}/2n_i)^2+\exp(-U_{NP})]^{1/2}+(P_{IM}/2n_i) \quad (14)$$

$$N_\infty/n_i=\exp(-U_N)=[(P_{IM}/2n_i)^2+\exp(-U_{NP})]^{1/2}-(P_{IM}/2n_i) \quad (15)$$

$$U_{GB}-U_{FB}-U_S=2U_{II}^{1/2}\times \mathrm{Sign}U_S\times F_{SI}(U_S,U_N,U_P) \quad (16)$$

$$[F_{SI}(U_S,U_N,U_P)]^2=[\exp(-U_S)+U_S-1]\exp(+U_P) +[\exp(+U_S)-U_S-1]\exp(-U_N) \quad (17)$$

The drain conductance or output conductance with input short-circuited is given by the derivative of I_D with respect to V_{DB} keeping V_{GB} and V_{SB} constant. Similarly, the transconductance is obtained. They are

$$g_{db}=\frac{\partial I_D}{\partial V_{DB}}=\frac{Z}{L}q\mu_n n_i L_{Di}\mathrm{Sign}U_{SL}\int_0^{U_{SL}}\frac{[\exp(+U)-1]\exp(-U_{DB})dU}{F_X(U,U_{NL},U_{PL})\sqrt{(P_{IM}/n_i)^2+4\exp(-U_{DB})}} \quad (18)$$

$$g_{mb}=\frac{\partial I_D}{\partial V_{GB}}=\frac{Z}{L}q\mu_n n_i L_{Di}\int_{U_{N0}}^{U_{NL}}\frac{[\exp(+U)-1]\exp(-U_N)dU_N}{F_{SI}(U_S,U_N,U_P)\,\mathrm{Sign}U_S\sqrt{U_{II}}\left[e^{U_P}(1-e^{-U_S})-e^{-U_N}(1-e^{U_S})\right]} \quad (19)$$

The multiplier or conductance normalization factor is $g_{norm}=(Z/L)\times q\mu_n n_i L_{Di}=I_{NORM}/(kT/q)$.

Because of the substantial numerical integration times, the above surface-potential-based equations of I_D, g_{db}, and $g_{mb,}$ of the long-wide-channel baseline transistor have not been used by compact modelers to develop short-narrow-channel and non-constant impurity concentration realistic compact models. However, due to their continuous property as a function of surface potential over the entire applied voltages without discontinuities, they are the bases for the second (next) generation of analytical compact models to include realistic geometries (short and narrow channels), spatially varying impurity concentrations, and nonequilibrium or hot carrier effects. These short-narrow-channel analytical compact models are then used to extract the numerical values of transistor parameters from experimental data, which are then used to generate the characteristics of the many different transistors in a circuit simulator such as SPICE to design optimized integrated circuits. For example, one of the first attempts to increase the computation speed, widely followed later, was given in 1978-Brews [12] who assumed two empirical approximations: (i) compressing the inversion layer into a conducting plane of zero thickness, called the charge sheet, which really corresponds to the mathematically rigorous delta-function approximation of the minority carrier charge density. As we shall see, it actually is not compressing the inversion charge distribution into a infinitesimal thin sheet, but rather raising the longitudinal electric field $E_Y(x,y)$ by flattening its x-distribution $|E_Y(x,y)| \sim< |E_Y(x=0,y)|$; and (ii) depleting the carrier concentration in the space-charge layer. {See equation (8) in 1978-Brews [12].} These approximations were recently given firmer theoretical grounds, but different device physics, in 2005-Jie-Sah [13] using the surface-potential-based space-charge theory obtained by Sah in 1996-Sah [14] which identified the channel current as a sum of four components, a drift current and a diffusion current that are carrier-space-charge-limited, and a drift current and a diffusion current that are bulk-impurity-charge-limited from the ionized impurities in bulk or the base-well region. This was known as the 4-component-drain-current theory, which was rigorously derived by Sah in 1996-Sah [14] from the 2-Dimensional DC steady-state carrier transport equations that include drift, diffusion, generation, recombination, trapping and tunneling known as the Shockley semiconductor equations. Three simple approximations can be used to reduce the numerical integration of the majority-carrier charge (or bulk-charge) contributions in the basewell-channel to simple analytical formulas. One of those gives mathematically results identical to the 1978-Brews empirical approximation, but different in device physics and mathematical rigor, and a second is the one commonly used by the inversion charge modelers. These are listed below and labeled by their numerical Bulk Charge approximation indicators, which is in fact the only term that is approximated to give the compact models. We shall use $Q_B = Q_P$ interchangeable from now on, although Q_P (or Q_{PB} where the subscript B is the Bulk-Charge Approximation or Model indicator, B=1 to 9) was the notation used for the exact or self-consistent solution while Q_B was the bulk-charge used in earlier papers which neglected the equilibrium or flatband minority carrier concentration, hence, did not adhere strictly to the assumption of x-independence of the quasi-Fermi potential, resulting in imaginary x-component DC electric field near flatband [1].

$$\begin{aligned}
-Q_P &= q\int_0^\infty (P_B-P)dx = qn_iL_{Di}\int_0^{U_S}\frac{\exp(+U_P)[1-\exp(-U)]}{\mathrm{Sign}U_S\times F_X(U,U_N,U_P)}dU \\
-Q_{PB} &= qn_iL_{Di}\mathrm{Sign}U_S\int_0^{U_S}\frac{d\{\exp(+U_P)[U-1+\exp(-U)]\}}{\sqrt{\exp(+U_P)[U-1+\exp(-U)]+\exp(-U_N)[\exp(+U)-1-U]}} && B=9 \\
&\cong qn_iL_{Di}\mathrm{Sign}U_S\times 2\sqrt{\exp(+U_P)\times[U_S-1+\exp(-U_S)]} && B=3 \\
&\cong qn_iL_{Di}\mathrm{Sign}U_S\times 2\sqrt{\exp(+U_P)\times|U_S-1|} && B=2 \\
&\cong qn_iL_{Di}\mathrm{Sign}U_S\times 2\sqrt{\exp(+U_P)\times|U_S|} && B=1
\end{aligned} \quad (20)$$

The multiplier or charge normalization factor is $Q_{NORM} = qn_iL_{Di} = I_{NORM}/[(Z/L)\times D_n] = 5.37\times10^{-12}$ C/cm^2 = 33.5×10^6q/cm^2 for intrinsic silicon at T=300K.

The induced electron charge densities $Q_{NB} = \int q(N-N_B)dx$ for the three bulk charge approximation (B=1, 2, 3) can be obtained from Eqs. (20) and (21) which is derived using the voltage equation (16):

$$\begin{aligned}
\int_0^{U_S}\frac{\exp(-U_N)[\exp(+U)-1]}{\mathrm{Sign}U_S\times F_X(U,U_N,U_P)}dU &= 2\times\mathrm{Sign}U_S\times F_{SI}(U_S,U_N,U_P)+\int_0^{U_S}\frac{\exp(+U_P)[\exp(-U)-1]}{\mathrm{Sign}U_S\times F_X(U,U_N,U_P)}dU \\
&= \frac{U_{GB}-U_{FB}-U_S}{\sqrt{U_{II}}}-\int_0^{U_S}\frac{\exp(+U_P)[1-\exp(-U)]}{\mathrm{Sign}U_S\times F_X(U,U_N,U_P)}dU
\end{aligned} \quad (21)$$

$$\begin{aligned}
\frac{-Q_{NB}}{Q_{NORM}} &= -\int_0^{U_S}\frac{\exp(-U_N)[\exp(U)-1]}{\mathrm{Sign}U_S\times F_X(U,U_N,U_P)}dU && B=0 \\
&= -2\mathrm{Sign}U_S\times F_{SI}(U_S,U_N,U_P)+\int_0^{U_S}\frac{\exp(U_P)[1-\exp(-U)]}{\mathrm{Sign}U_S\times F_X(U,U_N,U_P)}dU && B=9 \\
&\cong -2\mathrm{Sign}U_S\left\{F_{SI}(U_S,U_N,U_P)-\sqrt{\exp(U_P)\times[U_S-1+\exp(-U_S)]}\right\} && B=3 \\
&\cong -2\mathrm{Sign}U_S\left\{F_{SI}(U_S,U_N,U_P)-\sqrt{\exp(U_P)\times|U_S-1|}\right\} && B=2 \\
&\cong -2\mathrm{Sign}U_S\left\{F_{SI}(U_S,U_N,U_P)-\sqrt{\exp(U_P)\times|U_S|}\right\} && B=1
\end{aligned} \quad (22)$$

Our previous seven-digit numerical designation is used here to label the approximations of these baseline compact models, YYXXFRB. It was introduced to simplify curve labels and to give at-one-glance (A1G) the assumptions made in each of the compact models [1]. YY is the year

when the y-equation or current-equation was first used, for examples: (i) YY=66 for the 1966 Pao-Sah 1-term drain current formula with the double-integration of the product of the excess electron charge [N(x,y)−N(x=∞,y)] times the gradient of electrochemical potential $\partial U_{NP}/\partial y$ transformed from dxdy to $dU(x,y)dU_{NP}(y)$, which was introduced by Sah in 1966 [6], and (ii) YY=96 for the 1996-Sah 2-term (drift and diffusion) 4-component (space-charge and bulk-charge) rigorously derived drift-diffusion formula [14]. XX is the year when the x-equation or voltage equation was first used, for examples: (i) XX=65 for the 1965 Sah-Pao voltage-equation derived by Sah in 1964 and first presented and used in 1965 [5], which was not self-consistent and gave imaginary DC electric field near flatband and (ii) XX=04 for the voltage equation derived by Sah in 2004 that determined and removed the cause of the imaginary DC electric field near flatband {See reference [31] cited in [1].}, such as in YYXX=6604 and 9604. In the YYXXFRB label, F = 0 or 1 for the absence or presence of the flatband reference current, or the term $N_\infty = N(x=\infty,y)=N_B(y)$ in the inversion charge integral, Q_N, whose presence in (11) eliminates the unbounded flatband output or drain-source channel current. The Remote charge-neutrality boundary conductions are denoted by R = 1, 2, 3 which indicate respectively the multiplication of channel voltage exponential $\exp(-U_{NP})$ to one, two, or three minority or inversion carrier terms in (10). R=3 is the self-consistent case given in 2004-Sah [1] and used throughout this paper. R=2 is the inconsistent boundary condition, resulting in imaginary near-flatband electric field, introduced in 1965-Sah-Pao [5] and used by all subsequent compact model developers since 1978-Brews [12]. The accuracy of using R=1 have not been tested. B designates the exact and approximate bulk-charge formulas. B = 9 is for evaluation the 1-D and 2-D integral numerically, hence 'exact'. For the 1966-Pao-Sah 2-D integration [6], the only assumption is the y-independent quasi-Fermi-potentials of electrons and holes, which gave (12) for the drain current and (18) and (19) for drain-conductance and transconductance. For the 1996-Sah 4-component model, B=9 means that the 1-D and 2-D integrals are all numerically integrated exactly, except the 2-D integral accounting for the bulk-charge-reduction of the drift current which can only be numerically integrated in (x,y) or (U,U_{NP}) by assuming the x-independence of the y-electric field for the y-integration, The three (B=1, 2, 3) surface-potential-based bulk-charge approximations are defined in (20). In the following, we will give a brief derivation of the 'exact' integral model (9604139) and the three analytical compact models (9604133, 9604132, and 9604131).

The equilibrium or flat-band minority carrier concentration N_∞ is subtracted from the total electron concentration N in (4) to avoid unbounded I_D near and at flatband. This gives the two-mechanism (drift and diffusion) drain current equation:

$$I_D=-\int_z\int_y\int_x J_{Ny}(x)\,dx\,(dy/L)dz$$
$$= Z/L\int_y\int_x q\mu_n[N(x,y)-N(x=\infty)][\partial V(x,y)/\partial y]dxdy$$
$$-Z/L\int_y\int_x qD_n\partial[N(x,y)-N(x=\infty)]/\partial y dxdy \quad (23)$$

Using the approximation $\partial V(x,y)/\partial y \approx \partial V(0,y)/\partial y$, which is the x-independence approximation of the y-component of the electric field in Equation (220.24) of [1], rather than the delta-function approximation of the electron charge density in the 1978-Brews charge-sheet model [12], we obtain the 2-D numerical integral for the drift term, 139P0. The 1-D numerical integral for the diffusion term, 139D0, does not require any assumption. These give

$$I_D=I_{NORM}\times(139P0+139D0) \quad (24)$$

$$139P0=\int_{U_{SB}}^{U_{DB}}\frac{\partial U_S}{\partial U_{NP}}\int_0^{U_S}\frac{\exp(-U_N)[\exp(+U)-1]}{SignU_S\times F_X(U,U_N,U_P)}dUdU_{NP} \quad (25)$$

using $E_Y(x,y)\cong E_Y(x=0,y)$

$$139D0=\int_0^{U_{S0}}\frac{\exp(-U_{N0})[\exp(+U)-1]dU}{SignU_{S0}\times F_X(U,U_{N0},U_{P0})}-\int_0^{U_{SL}}\frac{\exp(-U_{NL})[\exp(+U)-1]dU}{SignU_{SL}\times F_X(U,U_{NL},U_{PL})} \quad (26)$$

Using the x- or voltage-equation (16) and (21) in the inner integral of the 2-D drift component 139P0, (25), and the diffusion component 139D0, (26), then we obtain the 1996-Sah 4-component current equations [14] listed below.

Compact Model YYXXFRB=9604139 (B=9)

$$\mathbf{I_D = I_{NORM}\times(139P3 + 139D3)}$$
$$\mathbf{= I_{NORM}\times(139P1+139P2 + 139D1+139D2)} \quad (27)$$

$$\mathbf{139P3 = 139P1 + 139P2} \quad (28)$$

$$139P1=[(U_{GB}-U_{FB}-U_{S0})^2-(U_{GB}-U_{FB}-U_{SL})^2]/(2U_{II}^{1/2})$$
carrier space-charge term (29)

$$139P2=-\int_{U_{SB}}^{U_{DB}}\frac{\partial U_S}{\partial U_{NP}}\int_0^{U_S}\frac{\exp(U_P)[1-\exp(-U)]}{SignU_S\times F_X(U,U_N,U_P)}dUdU_{NP}$$
ionized impurity charge or bulk-charge term (30)

$$\mathbf{139D3 = 139D1 + 139D2} \quad (31)$$

$$139D1=(U_{SL}-U_{S0})/U_{II}^{1/2}$$
carrier space-charge term (32)

$$139D2=\int_0^{U_{SL}}\frac{\exp(U_{PL})[1-\exp(-U)]dU}{SignU_{SL}\times F_X(U,U_{NL},U_{PL})}-\int_0^{U_{S0}}\frac{\exp(U_{P0})[1-\exp(-U)]dU}{SignU_{S0}\times F_X(U,U_{N0},U_{P0})}$$
ionized impurity charge or bulk-charge term (33)

Note, the two carrier space-charge components, drift 139P1 and diffusion 139D1, are independent of the impurity charge and are exact analytical solutions. Therefore, they are universal for all surface-potential-based compact models that contain analytical bulk-charge approximations, i.e., 13BP1=139P1 and 13BD1=139D1 where B=1, 2, and 3 and other values, (4,5,6,7,8), reserved for faster and more accurate new compact models. However, 139P2 needs to be transformed into the sum of two integrals in order to overcome numerical accuracy limit of the IMSL integration subroutines. The 4-component current formulas for the compact models B=1, 2, and 3 are obtained from (20). The B=2 approximation was used by 1978-Brews. The B=1 is a approximation commonly used by the inversion charge models. These are summarized in the following paragraphs.

Compact Model YYXXFRB=9604131 (B=1)

$$I_D=I_{NORM}\times(131P3+131D3)=I_{NORM}\times(139P1+131P2+139D1+131D2) \quad (34)$$
$$131P3=139P1+131P2 \quad (35)$$
$$131P2=-(4/3)\times\{\exp(U_{PL}/2)\times|U_{SL}|^{3/2}-\exp(U_{P0}/2)\times|U_{S0}|^{3/2}\} \quad (36)$$
$$131D3=139D1+131D2 \quad (37)$$
$$131D2=2SignU_{S0}\times\{\exp(U_{PL}/2)\times|U_{SL}|^{1/2}-\exp(U_{P0}/2)\times|U_{S0}|^{1/2}\} \quad (38)$$

Compact Model YYXXFRB=9604132 (B=2)

$$I_D=I_{NORM}\times(132P3+132D3)=I_{NORM}\times(139P1+132P2+139D1+132D2) \quad (39)$$
$$132P3=139P1+132P2 \quad (40)$$
$$132P2=-(4/3)\times\{\exp(U_{PL}/2)\times|U_{SL}-1|^{3/2} -\exp(U_{P0}/2)\times|U_{S0}-1|^{3/2}\} \quad (41)$$
$$132D3=139D1+132D2 \quad (42)$$
$$132D2=2\times SignU_{S0}\times\{\exp(U_{PL}/2)\times|U_{SL}-1|^{1/2} -\exp(U_{P0}/2)\times|U_{S0}-1|^{1/2}\} \quad (43)$$

Compact Model YYXXFRB=9604133 (B=3)

$$I_D=I_{NORM}\times(133P3+133D3)=I_{NORM}\times(139P1+133P2+139D1+133D2) \quad (44)$$
$$133P3=139P1+133P2 \quad (45)$$
$$133P2=-\int_{U_{S0}}^{U_{SL}}SignU_S\,2\sqrt{\exp(+U_P)\left[\exp(-U_S)-1+U_S\right]}\,dU_S \quad (46)$$
$$\cong -\frac{4}{3}\left\{\exp(U_{PL}/2)\left[\exp(-U_{SL})-1+U_{SL}\right]^{3/2}-\exp(U_{P0}/2)\left[\exp(-U_{S0})-1+U_{S0}\right]^{3/2}\right\}$$
$$133D3=139D1+133D2 \quad (47)$$
$$133D2=2\times SignU_{S0}\times\{\exp(U_{PL}/2)\times[U_{SL}-1+\exp(-U_{SL})]^{1/2} -\exp(U_{P0}/2)\times[U_{S0}-1+\exp(-U_{S0})]^{1/2}\} \quad (48)$$

Taking derivatives of drain current and using the derivatives of U_{SL} and U_{S0} listed below, the output conductance and transconductance of these three compact models are readily obtained.

$$\frac{\partial U_{S0}}{\partial U_{DB}}=0 \quad (49)$$
$$\frac{\partial U_{SL}}{\partial U_{DB}}=\frac{\exp(U_{DB})\left[\exp(U_{SL})+\exp(U_{SL})-2\right]signU_{SL}\sqrt{U_{II}}}{\sqrt{(P_{IM}/n_i)^2+4e^{-U_{DB}}}\left\{F_{SI}(U_{SL},U_{NL},U_{PL})+signU_{SL}\sqrt{U_{II}}\left[e^{-U_{NL}}(e^{U_{SL}}-1)-e^{U_{PL}}(e^{-U_{SL}}-1)\right]\right\}} \quad (50)$$
$$\frac{\partial U_{S0}}{\partial U_{GB}}=\frac{F_{SI}(U_{S0},U_{N0},U_{P0})}{F_{SI}(U_{S0},U_{N0},U_{P0})+signU_{S0}\sqrt{U_{II}}\left[e^{-U_{N0}}(e^{U_{S0}}-1)-e^{U_{P0}}(e^{-U_{S0}}-1)\right]} \quad (51)$$
$$\frac{\partial U_{SL}}{\partial U_{GB}}=\frac{F_{SI}(U_{SL},U_{NL},U_{PL})}{F_{SI}(U_{SL},U_{NL},U_{PL})+signU_{SL}\sqrt{U_{II}}\left[e^{-U_{NL}}(e^{U_{SL}}-1)-e^{U_{PL}}(e^{-U_{SL}}-1)\right]} \quad (52)$$

Induced or Excess Charge Densities

Figure 1 gives the induced or excess carrier charge densities (flatband as the reference) of the three compact models (B=3, 2, 1) and their accuracies. The induced electron charge densities Q_{NB}(B=3,2,1) deviate significantly from the 'exact' integration solution, Q_{N9}(B=9), in the accumulation (V_{GF} <0) range, while Q_{N3}(B=3) matches Q_{N9} well in the V_{GF}>0 range. These large deviations prompted us to seek a better approximation or compact model. For this purpose, we tried the 1961-Sah 3-layer approximation which was first used in the 1965-Sah-Pao [5] bulk-charge model and gave good results. This will be designated as compact model B=6, with $Q_{NB}=Q_{N6}$. The analyses and the solutions are summarized in the following paragraphs.

$$\frac{-Q_{N6}}{Q_{NORM}}=-\int_0^{U_S}\frac{\exp(-U_N)\left[\exp(U)-1\right]}{SignU_S\times F_X(U,U_N,U_P)}dU \quad \text{when } U_S<0 \quad (53)$$
$$\cong\int_0^{U_S}\frac{\exp(-U_N)\left[\exp(U)-1\right]}{\sqrt{\exp(U_P)\left[\exp(-U)-1+U\right]}}dU, \quad U_1=-2-\log_e(1-U_1)$$
$$\cong\exp(-U_N-U_P/2)\left\{2\int_0^{U_1}\exp(U)d\sqrt{\exp(-U)-1+U}-\int_{U_1}^{U_S}\exp(U/2)dU\right\}, \text{when } U_S<U_1$$
$$=2\exp(-U_N-U_P/2)\int_0^{U_S}\exp(U)d\sqrt{\exp(-U)-1+U}, \text{when } 0>U_S>U_1$$

which is further approximated as follows

$$\int_0^{U_S}\exp(U)d\sqrt{\exp(-U)-1+U}$$
$$=\exp(U_S)\sqrt{\exp(-U_S)-1+U_S}-\int_0^{U_S}\exp(U)\sqrt{\exp(-U)-1+U}dU$$
$$\cong\exp(U_S)\sqrt{\exp(-U_S)-1+U_S}-\int_0^{U_S}\exp(U)\sqrt{U^2/2-U^3/6}dU$$
$$=\exp(U_S)\sqrt{\exp(-U_S)-1+U_S}-SignU_S/\sqrt{2}\times\left\{\left[-U_S^2/6+4/3\times(U_S-1)\right]\exp(U_S)+4/3\right\} \quad (54)$$

Then the analytical approximations for the three U_S ranges or three layers of Q_{N6} of (53) are given by:

$$Q_{N6}(U_S,U_N,U_P)/(-2Q_{norm})$$
$$=\exp(U_P/2)\,[U_S-1+\exp(-U_S)]^{1/2}-F_{SI}(U_S,U_N,U_P), \text{ when } U_S\geq 0 \quad (55a)$$
$$=\exp(-U_N-U_P/2)\{\exp(U_S)\,[\exp(U_S)-1+U_S]^{1/2} +[(-U_S^2/6+4U_S/3-4/3)\exp(U_S)+4/3]/\sqrt{2}\}, \text{ when } 0>U_S\geq U_1 \quad (55b)$$
$$=\exp(-U_N-U_P/2)\{\exp(U_1)\,[\exp(U_1)-1+U_1]^{1/2} +[(-U_1^2/6+4U_1/3-4/3)\exp(U_1)+4/3]/\sqrt{2} +\exp(U_1/2)-\exp(U_S/2)\}, \text{ when } U_S<U_1 \quad (55c)$$

Figure 1b shows that Q_{N6} matches the exact Q_{N9} well in all gate voltage ranges. The new analytical compact model B=6 is then

Compact Model YYXXFRB=9604136 (B=6)

$$I_D=I_{NORM}\times(136P3+136D3) \quad (56)$$
$$136P3=133P3 \text{ when } U_S>0, \quad (57a)$$
$$=0 \text{ when } U_S\leq 0 \quad (57b)$$
$$136P2=136P3-139P1 \quad (58)$$
$$136D3=133D3 \text{ when } U_S>0, \quad (59a)$$
$$=I_{NORM}/Q_{NORM}\times\{Q_{N6}(U_{S0},U_{N0},U_{P0})-Q_{N6}(U_{SL},U_{NL},U_{PL})\}| \text{ when } U_S\leq 0 \quad (59b)$$
$$136D2=136D3-139D1 \quad (60)$$

3 ACCURACY OF THE BASELINE COMPACT MODELS

In this section and its subsections, we present the numerical results of the transfer and the output characteristics of the drain or channel current, $I_D(V_{GF},V_{DS}$=constant,V_{SB}=constant) and $I_D(V_{DS},V_{GF}$= constant,V_{SB}=constant). We also present the numerical results of the transconductance and drain or output conductance as a function of gate voltage, $g_{mb}(V_{GF},V_{DS}$=constant,V_{SB}=constant) and $g_{db}(V_{GF},V_{DS}$= constant,V_{SB}=constant), and as a function of the drain

voltage $g_{mb}(V_{DS},V_{GF}$=constant,V_{SB}=constant), and $g_{db}(V_{DS}$, V_{GF}=constant,V_{SB}=constant). $V_{GF}=V_{GB}-V_{FB}$ is the gate voltage relative to the flatband gate voltage, using the basewell or bulk=body as the voltage reference node. We assume an ideal n-inversion-channel MOS transistor without a p/n-junction-isolated p-basewell on the p-body, designated by the node B. We computed the current-voltage (I-V) and conductance-voltage (g-V) characteristics of the four analytical approximations or compact models, designated by B=1, 2, 3, and 6. We also computed their percentage deviations from the 'exact' (numerically integrated) B=9 model. The results are graphically illustrated in the following discussions. The B=9 model itself is not quite exact since the charge-sheet approximation [Note that this is really not the 1978-Brews empirical charge-sheet approximation. It is actually the x-independence approximation of the y-component of the electric field $E_Y(x,y)\sim E_Y(x=0,y)$.] or correctly, the x-independent y-component-electric-field approximation is used to make the current-equation or y-equation numerically integratable as explained the preceding section. The properties of the ideal inversion n-channel transistors assumed are: P_{IM}(say Boron) = 1.0×10^{18} cm^{-3}, gate oxide (SiO_2) thickness X_{OX} = 2.0 nm, and channel aspect ratio (width/length) = Z/L = 1, or the current is per square. Results of only the metal gate are presented assuming an aluminum metal, using the experimental aluminum vacuum workfunction Φ_{AL}=4.679eV with an estimated experimental SiO_2 electron affinity χ_{SiO2} = 0.9 to 1.0eV {See Table 413.1 on p.150 of 1993-Sah-FSSE-SG [15].} although the silicon MOS designers have used the value 4.2eV for the Al/SiO_2 barrier height. {See Table in section 563 on p.220 of [15].} This uncertainty only shifts the flatband gate voltage, V_{FB}, (by about 4.679−0.900− 4.200 = −0.421V) not the features and results, since all use the gate voltage relative to the flatband, $V_{GB}-V_{FB}=V_{GF}$.

In all the transfer-characteristic (vs V_{GF}) figures to be described, three light vertical lines are drawn to show the amount of surface band bending (U_F and $2U_F$) at the p-base-edge of the source n/p junction for the corresponding gate voltages. They are labeled $U_S=U_{S0}$= 0, U_F, $2U_F$ for flatband (U_{S0}=0,V_{GF}=0V), intrinsic surface and subthreshold voltage ($U_{S0}=U_F$,$V_{GF}=V_{Gsub}$), and on-set of strong surface inversion ($U_{S0}=2U_F$,$V_{GF}=V_{Gth}$). These three vertical lines divide the gate voltage range (−3V, 4V) into the four device-physics-useful operational gate voltage ranges which are: the accumulation range ($U_{S0}<0$), the deep-subthreshold range ($0<U_{S0}<U_F$), the subthreshold range ($U_F<U_{S0}<2U_F$), and the strong inversion range ($U_{S0}>2U_F$).

3.1 Induced electron and hole charge densities

Figures 1(a) to 1(d) show the induced or excess electron and hole charge densities (relative to flatband) at the p-basewell edge (y=0) of the n++Source/p-Basewell junction space-charge region at the SiO_2/Si interface (x=0) which is the origin of our coordinate system, (x=0,y=0). These figures give both the induced electron and hole charge densities for the four compact model approximations, B=1,2,3,6, Q_{NB}(y=0) and Q_{PB}(y=0), in Figs. 1(a) and (c), and also their percentage deviations from the exact numerical-integration non-compact model B=9 in Figs. 1(b) and (d). The goodness of the approximation models is different for the induced hole and electron charges.

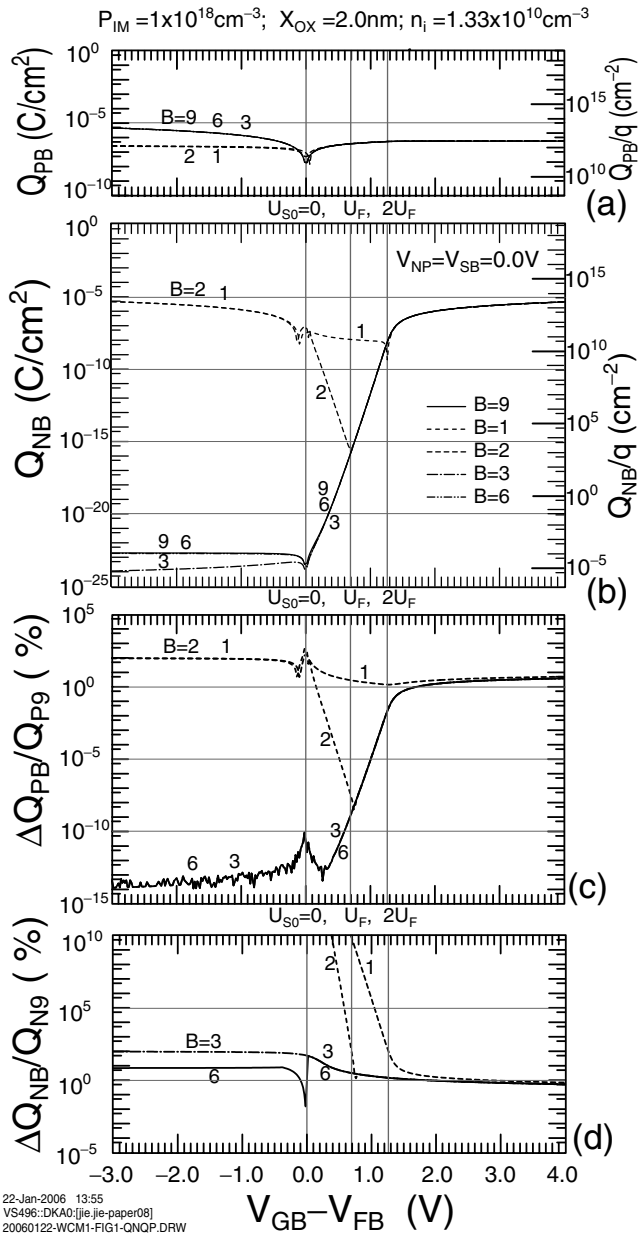

Figure 1: Variation of excess carrier charge densities with applied gate voltage, (a) Holes, and (b) Electrons. And the percentage deviation of (c) Holes and (d) Electrons of the two integration models 6604139 and 9604139, and of the four compact approximation models, 960413B (B=1,2,3,6).

Generally, the four approximations are adequately good in the strong inversion range, $V_{GF}>V_{GFth}$=+1.262V, but are

poor in the subthreshold range and increasingly worsen in the deep subthreshold range and becoming rather bad in the accumulation range for B=1,2,3 (1 is the worse, 2 somewhat better, and 3 still better), except the specially designed 3-layer compact model B=6 which is adequate (< ~10%) for all four ranges of V_{GF}. These charge density illustrations are useful for developing better approximations for the inversion charge compact models and charge-controlled capacitance modeling for analog and RF circuit designs.

3.2 Transfer characteristics

Figure 2(a) gives the transfer characteristics $I_D(V_{GB}-V_{FB})$ of all six models: the two exact numerical-integration models (B=0,9) and the four 4-component analytical compact models (B=1,2,3,6). Figures 2(b) and 2(c) give the log and linear percentage deviation of I_D of the four 4-component compact models (B=1,2,3,6) from the exact numerical-integration 4-component model B=9, $\Delta I_{DB}/|I_{D9}|$, and also the deviation of B=9 from B=0, $\Delta I_{D9}/|I_{D0}|$. The two 'exact' numerical-integration solutions are: **(i)** B=0 for 6604139, not using the 1965-Sah-Pao [5] x-equation (R=2) but using the corrected 2004-Sah remote boundary condition (R=3) [1], and using the 1966-Pao-Sah [6] 2-D integration y-equation or current equation with the flatband current subtracted, and **(ii)** B=9 for 9604139 using the 1996-Sah 4-component 1-D and 2-D integration equations [14], not the 1978-Brews charge-sheet approximation [1, 12] but the x-independence approximation of the

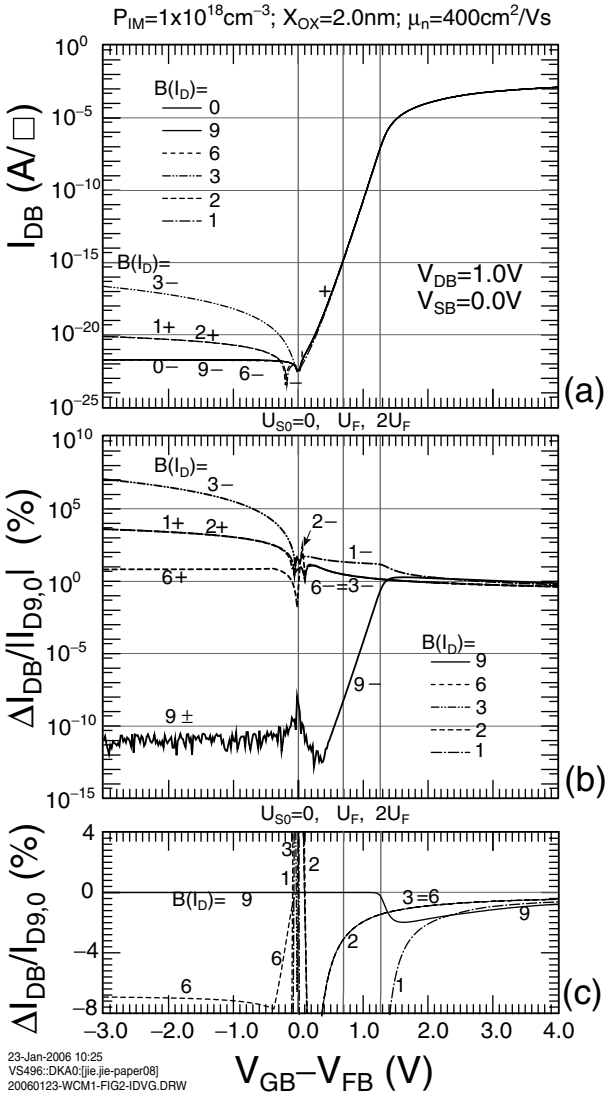

Figure 2: DC transfer characteristics (I_{DB}-V_{GF}) of the two integration (6604139 and 9604139) and four analytical compact-approximation (960413B, B=1,2,3,6) models. (a) Drain current. Percentage deviation of drain current (b) Semilog and (c) Linear.

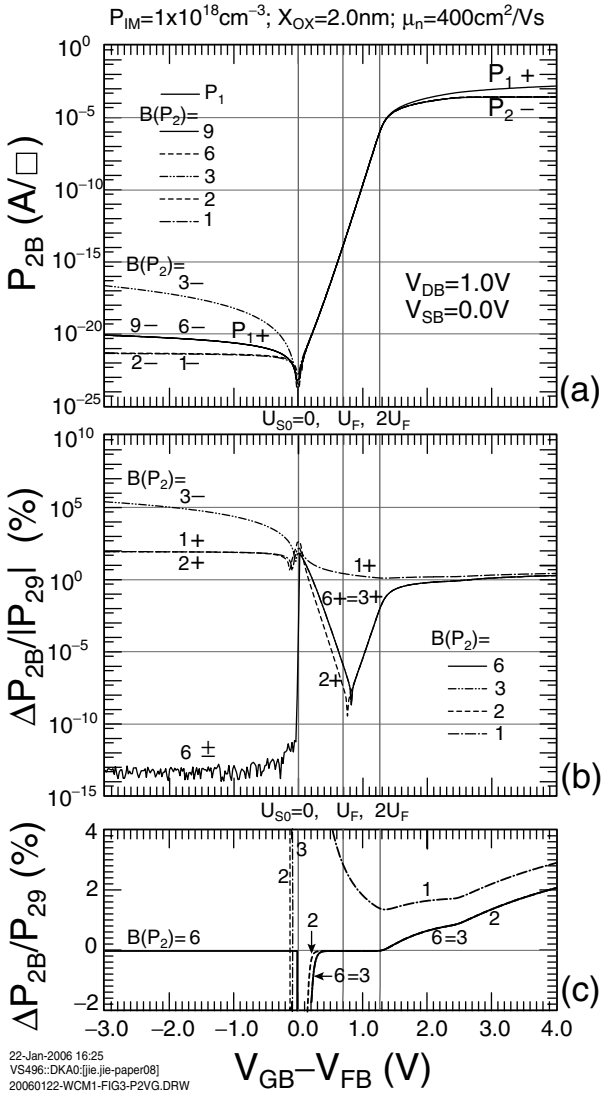

Figure 3: Variation of the bulk-charge reduction of drift component currents in the 4-component model, P_{2B}, with applied gate voltage of the one integration (B=9) and four analytical compact-approximation (B=1,2,3,6) models. (a) P_{2B}. Percentage deviation of P_{2B} from the integration model P_{29} (b) Semilog and (c) Linear.

longitudinal electric field, $|E_Y(x,y)| \sim< |E_Y(x=0,y)|$, revealing the origin of $I_D(9604139) < I_D(6604139)$.

Figure 2(a) shows the success of computing the extremely small currents, 10^{-23} to 10^{-20} A/□ in the accumulation range, $V_{GF}<0$, which may have not been attained by other authors.

Since B=9 (9604139) is the baseline to compute the deviation of the four analytical compact models 960413B (B=1,2,4,6), we need to first ascertain the accuracy of B=9 baseline model. This is demonstrated by computing the deviation of B=9 from the exact model B=0 (6604139). As expected, the deviation is small, but not zero due to the x-independence approximation $|E_Y(x,y)| \sim < |E_Y(x=0,y)|$. Indeed it is very small, as shown in Fig.2(b), in the accumulation range, $\Delta I_{D9}/|I_{D0}|<\pm 1\times 10^{-11}\%$ for $V_{GF}<0$, and the subthreshold range $\Delta I_{D9}/|I_{D0}|<-0.5\%$ for $V_{GF}< +1.262$V ($U_{S0}<2U_F$). Then it rises, shown in the linear expanded scale in Fig..2(c), and peaks to about −2% at V_{GF}=+1.4V and $U_{S0}\sim 2U_F+2$, i.e. the onset of strong inversion. This negative peak was also reported previously by us [1,13]. It is not expected if B=9 were truly exact. Thus, the origin of this smaller I_D of B=9 compared with that of B=0 computed from 1966-Pao-Sah 2-D using 1996-Sah must be due to the x-independence approximation of the longitudinal (y-axis) component of the electric field in the y-integration which gives too high a contribution of the bulk-charge-reduction ($P_2<0$) of the drift current in the x>0 region. This was not recognized previously in the charge sheet assumption made in 1978-Brews. The 1978-Brews terminology of charge-sheet is erroneous because it implied lumping the distributed electron charges (x=0 to x=∞) into a thin sheet at x=0 where the y-electric field is the highest, which would then overestimate the electron drift current contribution from electron charges that were originally at x>0 where the y-electric fields are lower. A numerical proof of this analytical and device-physics-based proof will require 2-D (x,y) solutions, which will be attempted in a future report.

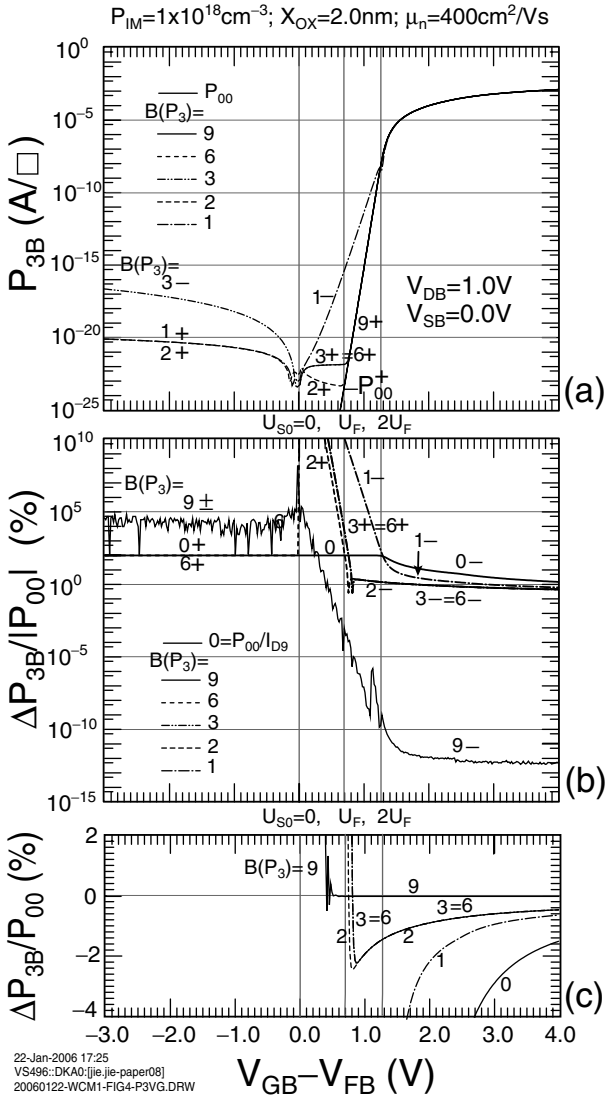

Figure 4: Variation of drift current, $P_{3B}=P_{1B}+P_{2B}$, with applied gate voltage of the one integration (B=9) and four analytical compact-approximation (B=1,2,3,6) models. (a) P_{3B}. Percentage deviation of P_{3B} from the integration model P_{00} (b) Semilog and (c) Linear.

Next, we examine the accuracy of the deviation from B=9 of the four analytical compact models, B=1,2,3,6. Figure 2(c) shows that the three compact models B=2,3,6 give excellent results (<−3%) in the inversion and subthreshold range, $V_{GF}\equiv V_{GB}-V_{FB}>+0.70$V ($U_{S0}>U_F$), while the simplest compact model, B=1, which is commonly used by the inversion charge models, starts to diverge rapidly (smaller) still in the inversion range, below about V_{GF}=+1.5V.

Figure 2(b) shows that the accuracy of all three simple compact models (B=1,2,3) are very poor in the accumulation range $V_{GF}<0.0$V ($U_{S0}<0$). This is because the three electron charge density terms $[\exp(+U)-U-1]\times\exp(-U_N)$ in the normal or x-direct electric field, (13), $[F_X(U,U_N,U_P)]^2 = [\exp(-U)+U-1]\exp(+U_P)+[\exp(+U)-U-1]\exp(-U_N)$ are neglected when making the approximate analytical evaluation of (i) the 1-D bulk-charge integral of the x-integration to give the bulk-charge-enhanced diffusion current component and (ii) the 2-D (x,y)-integration to give the bulk-charge-reduced drift current component, even though the electron charge density, $Q_N(x,y)$ is so much smaller than the hole or bulk charge density, $Q_P(x,y)$, and the latter determines the electric field in the denominator of the x-integration, and even though $Q_N(x,y)$ is so squeezed into a thin sheet δ(x) at the SiO_2/Si interface as described by 1978-Brews but rather determined by the x-distribution of the y-component of the electric field along the channel current flow. An additional source of deviation was from keeping exp(−U) of the three hole concentration terms of (13) constant in the dU(x) and $dU_{PN}(y)$ or $dU_S(y)$ integration, such as those in (46) for $dU_S(y)$ integration, in order to give the analytical solution for B=1,2,3. To remedy this, the approximate analytical solution for B=6 is cooked up rigorously following the 3-

layer approximation method developed by Sah in 1961 for MOS capacitance-voltage calculation which was then used for MOS transistor in 1965-Sah-Pao [5]. This led to B=6 compact model given by (56) to (60).

In order to get a better understanding that could help to develop more accurate compact models, we shall use next several figures to get to the origins of the deviations. We notice on the onset that the deviations, recognized as early as the 1965-Sah-Pao [5] as indicated by the title of this 1965 article, are solely from the analytical approximations used to evaluate the two impurity bulk-charge integrals: the 1-D x-integration of the diffusion current (26) and 2-D (x,y) integrations of the drift current (25). Figures 3(a) shows the bulk-charge-reduced drift-current component P2B of all four compact models (B=1,2,3,6) and the reference or 'exact' integral model (B=9). As anticipated, the large deviations of the total drain or channel current of the four compact models shown in Figs.2(b) on semilog, and in 2(c) on linear axes, indeed originated from the bulk-charge term P2 as verified by the shape and magnitude of the percentage deviation curves of the four compact models shown in Figs.3(b) and 3(c). This is expected since the carrier space-charge term P1 is already analytical and hence no error since no analytical approximation to P1 was needed for compact modeling. Note especially the success of the new compact model B=6, which has extremely accurate P2 (note P2 is negative i.e. bulk-charge reduces drift current via threshold voltage shift first shown in 1965-Sah-Pao [5]) in the accumulation range with $\Delta P_{26}/P_{29} < \pm 10^{-13}$% shown in Fig.3(b) and < 2% in the deep subthreshold to the strong inversion ranges shown in Fig.3(c), which also shows that the new compact model B=6 is still inaccurate but only in a very small range near the flat-band $0<V_{GF}<+0.3$V where the asymptotic expansion about $U_S=0$ is made in the square root of the integrand of (57a) or (46) to make it integrable analytically. The error reaches ~100% (a factor of two off)

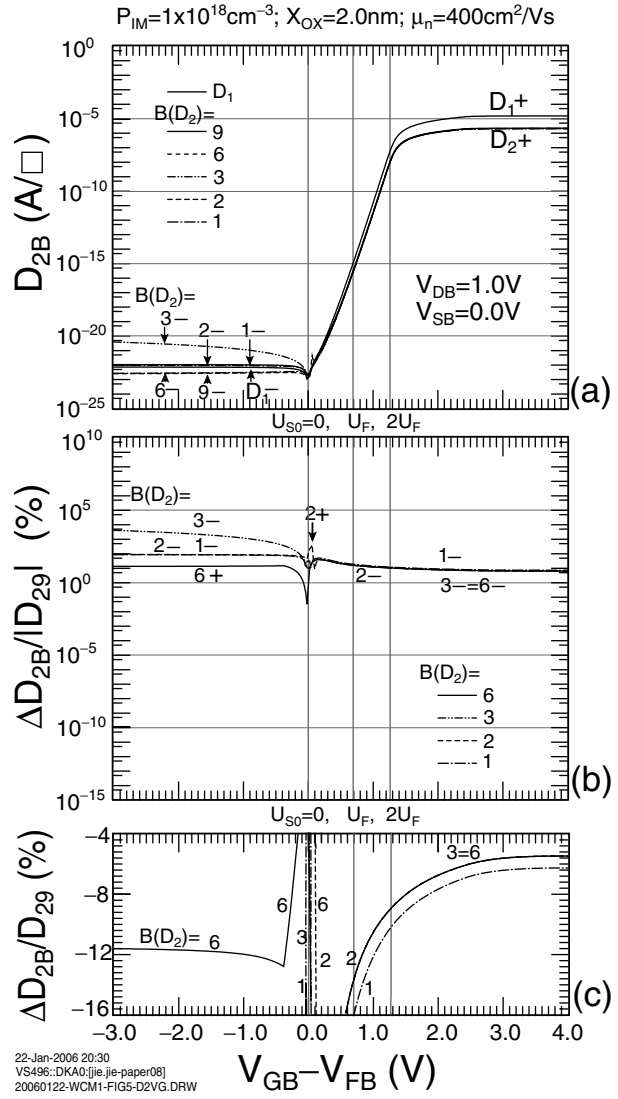

Figure 5 (a), (b), and (c). Same as Figure 3 but on the two diffusion component currents.

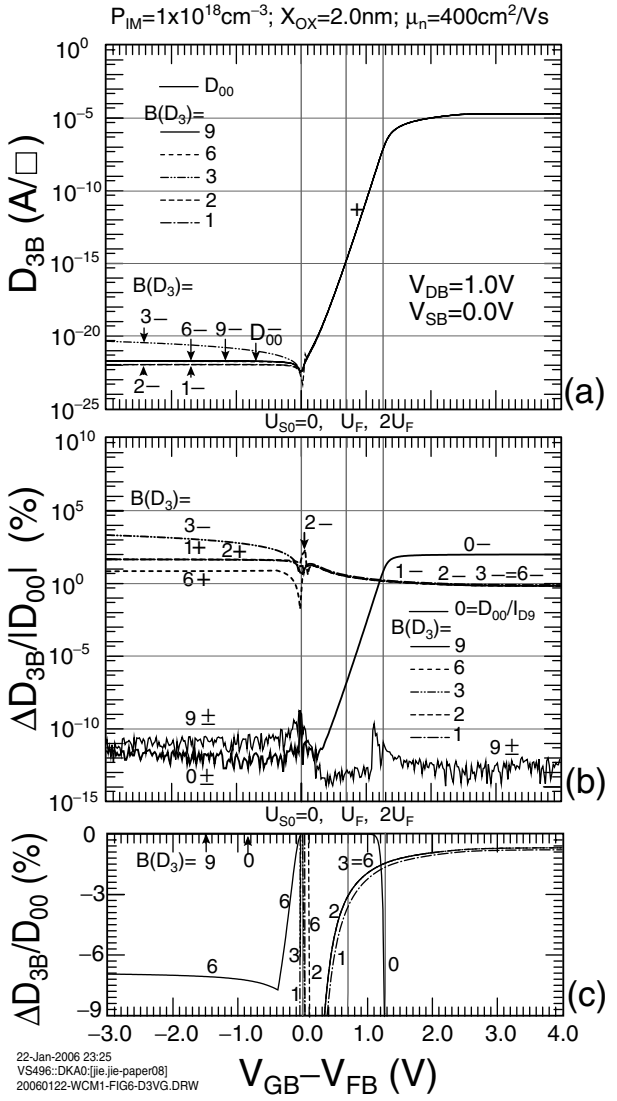

Figure 6: (a), (b), and (c). Same as Figure 4 but on the diffusion current.

at flat-band because of the three electron and three hole terms in the square root in the neglected denominator. However, this error in drift current at flatband is not much of a concern on the total current accuracy because blow threshold (including flatband), diffusion dominates over drift. Figure 3(a) also gives the carrier space-charge drift current component, P1, to show the nearly equal value and hence the cancellation of P1 and P2, making the analytical approximation and numerical computation difficult because of subtracting two small numbers ($<10^{-20}$), P1−(−P2)=P3, to give an even smaller number, P3 ($<<10^{-30}$) in Fig. 4(a).

Figures 4(a), 4(b) and 4(c) give another way to get the baseline (with the hope that some kinks and discontinuities could be easier discovered and eliminated in the earlier debugging of the FORTRAN), namely, using total drift current component P3B(B=9) from adding the integrated bulk-charge model P2B(B=9) to the exact analytical space-charge P1B(B=9), P3B=P1B+P2B (B=9). These are then compared with the numerically exact 1-term 2-D (x,y) integration of the total drift current, to be denoted by P00. Theoretically P00 must be equal to P39. But in practice, it is not, as demonstrated by the computed data and their random fluctuations which are labeled by P39/P00 and 100×[(P39/P00)−1] in Fig.4(b). The difference comes from numerical precision limits of both the computer hardware (64-bit ALPHA-station running 64-bit OpenVMS and 64-bit FORTRAN-90) and the software (64-bit FORTRAN-90 and the 32-bit IMSL Fortran integration subroutine). Figure 4(c) shows that the difference between B=0 and B=9 (the curve labeled by 9) is negligible, essential zero, from strong inversion (V_{GF}=+4V, $U_{S0}>2U_F+2$) down to deep subthreshold (V_{GF}=+0.5V, $U_{S0}\cong U_F/2$). The difference becomes large (>100%) only below this normal operation range and in accumulation. Figure 4(c) also shows that the total drift current, P36=P16+P26, of the new compact model, B=6, indeed gives excellent approximation to P00 anticipated from the analytical 3-layer approximation made to evaluate the 2-D P26 integral.

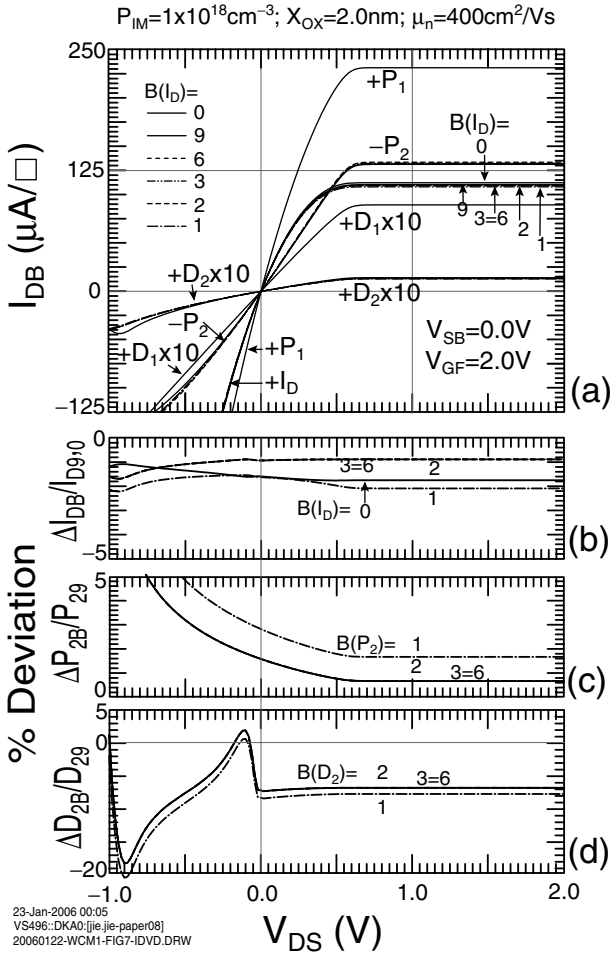

Figure 7: Output characteristics (Drain Current versus Drain Voltage) of the two integration and four analytical compact-approximation models in the strong inversion range V_{GF} =2.0V. Same as Figure 2 except here versus drain voltage. (a) I_{DB}. Percentage deviation, all in linear scale, of (b) total current from $I_{D9,0}$, (c) drift component, P_{2B} from P_{29} and (d) diffusion component, D_{2B} from D_{29}.

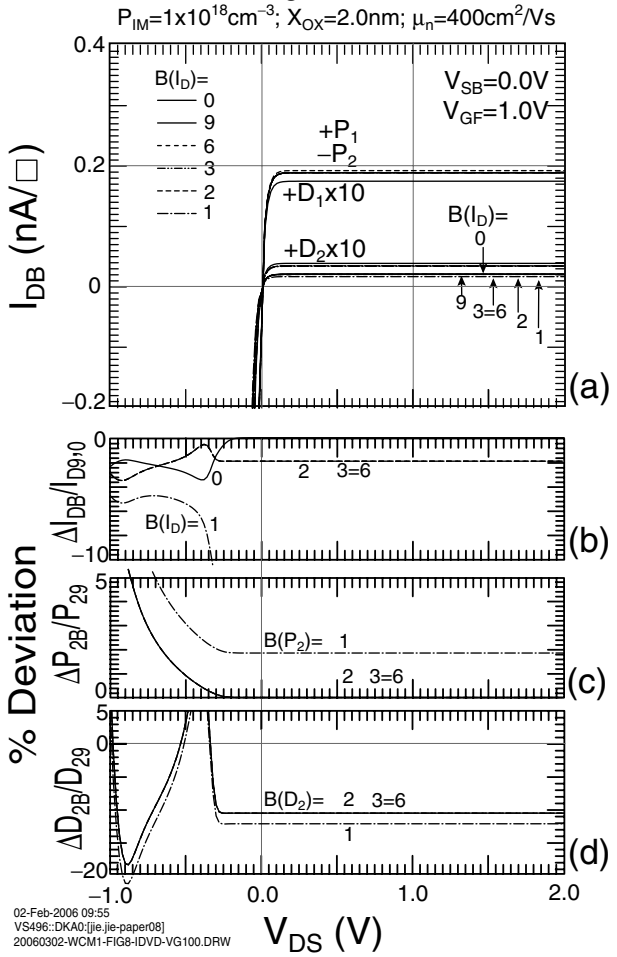

Figure 8: Output characteristics (Drain Current versus Drain Voltage) of the two integration and four analytical compact-approximation models in the subthreshold range V_{GF} =1.0V. Same as Figure 7 except V_{GF}.

Figures 5 and 6 show the two diffusion current components, space-charge-limited D1 and bulk-charge-enhanced D2, which are counter parts of Figs. 3 and 4 of the drift current components just discussed in the preceding paragraph. The conclusions are similar, noting also that diffusion current dominates below the threshold and in accumulation V_{GF}<+1.262V (U_{S0}<2U_F), and again the B=6 compact model gives excellent results from accumulation to subthreshold, continues into strong inversion range, except a small flatband voltage range, although the deviation of the diffusion current is larger in the accumulation range $|\Delta D_{36}|/D_{00}$ < |−8%| than that of the drift current in the inversion range $|\Delta P_{36}|/P_{00}$ < |−2.2%|.

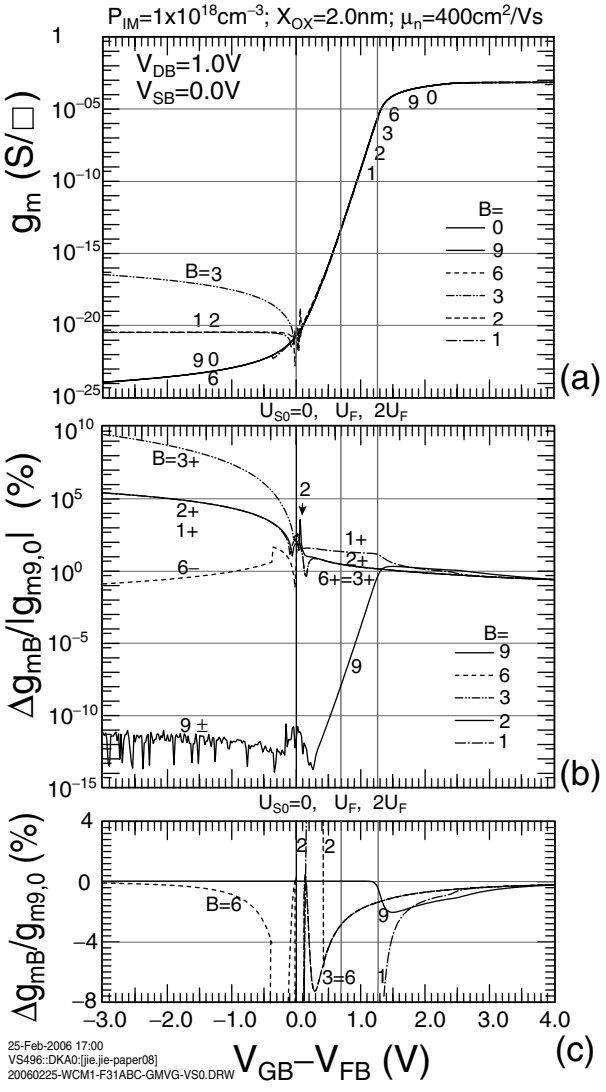

Figure 9 Transconductance vs gate voltage characteristics. (a) g_m. Percentage deviation from $g_{m9,0}$ (b) Semilog and (c) Linear.

3.3 Output Characteristics

Output characteristics of I_D versus V_{DB} are computed and presented in this section for one inversion point at V_{GF} ≡ V_{GB}−V_{FB} = +2.0V > V_{GF}-th(U_{S0}=2U_F)=+1.262V and V_{SB} = 0.0V in Figs.7(a)-7(d), and one subthreshold point at V_{GF} ≡ V_{GB}−V_{FB} = +1.00V at U_{S0}=3U_F/2 and V_{SB} = 0.0V in Figs.8(a)-8(d). Consider first the strong inversion point, V_{GF}=+2.0V, the four current components, D1, D2, P1 and P2, are shown Figs. 7(a) to 7(d). These include the four analytical compact models (B=1,2,3,6) and the two exact integration models (B=9 for 9604139 and B=0 for 6604139). The total current and its four components are shown in Fig. 7(a) with the two diffusion components (space-charge and bulk-charge limited, D1 and D2) amplified by 10X to give visibility since they are about ten

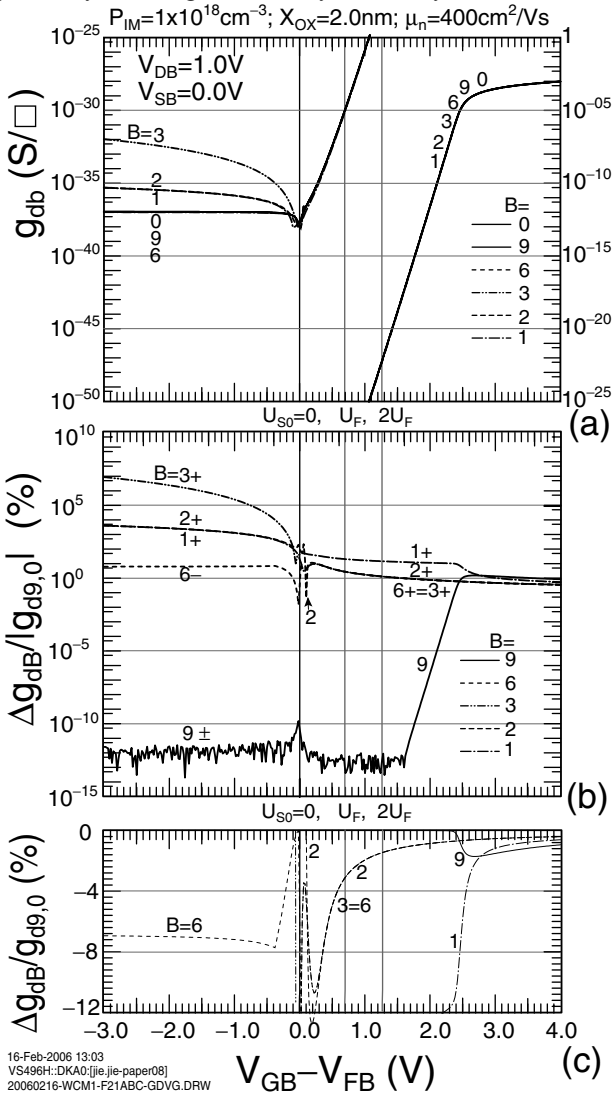

Figure 10: Drain or Output conductance versus gate voltage characteristics. (a) g_d. Percentage deviation from $g_{d9,0}$ (b) Semilog and (c) Linear.

times smaller in the inversion range (from using V_{GF}=+2.0V). Figure 7(b) gives the deviation of the total current of the four analytical compact models (B=1,2,3,6), the integrated 4-component baseline model (B=9), $\%\Delta D_{DB}/D_{D9}$, and also the deviation of B=9 (9604139) from B=0 (6604139, labeled by 0). Figures 7(c) shows the deviation of bulk-charge drift current component of the four analytical compact models (B=1,2,3,6) from that of the analytical baseline (B=9), $\%\Delta P_{2B}/P_{29}$, and Fig. 7(d), that of the bulk-charge diffusion component, $\%\Delta D_{2B}/D_{29}$. For this strong inversion point, V_{GF}=+2.0V > $V_{GF\text{-}th}$ (U_{S0}=2U_F) =+1.262V, as expected, these deviations are all small, even for the worse subthreshold-accumulation compact model, B=1, only about −2% for the total current, and 1.7% for the bulk-charge drift component P2. The −8% deviation for the bulk-charge diffusion component D2, shown in Fig. 7(d), is small in magnitude in the total drain current since in this range, drift dominates diffusion by more than 10 times as shown in Fig.7(a). Four similar figures, Fig.8(a)-(d), show the characteristics at the subthreshold point, V_{GF}=+1.0V, with a drain saturation current of about 10^{-10}A/□ and much sharper saturation at V_{DS} ~ 4kT/q ~ 0.1V, and also larger deviation of the analytical compact models.

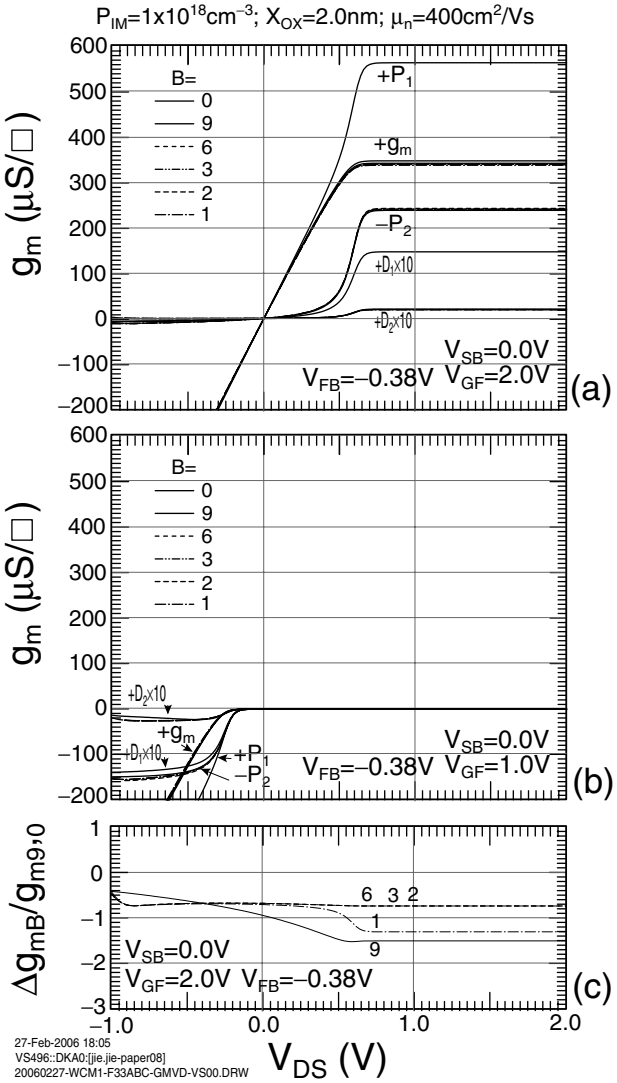

Figure 11: Transconductance versus drain voltage characteristics. (a) g_m. Percentage deviation from $g_{m9,0}$ (b) Semilog and (c) Linear.

3.4 Transfer-Output Conductance Characteristics

The transfer (transconductance) g_{mb} and output conductance characteristics g_{db} are shown in Figs. 9(a)-(c) and 10(a)-(c) as a function of gate voltage, $V_{GB} - V_{FB}$, and in Figs. 11(a)-(c) and 12(a)-(c) as a function of drain/source voltage, V_{DS} at zero body bias V_{SB}=0V. The main result is that there is no discontinuity in these derivatives. Another is the saturation of I_D or excellent exponential V_{DS} dependence of g_{db} at approximately V_{GS}≈V_{DS} as shown in Fig. 12(a). A third is the small deviation of B=6.

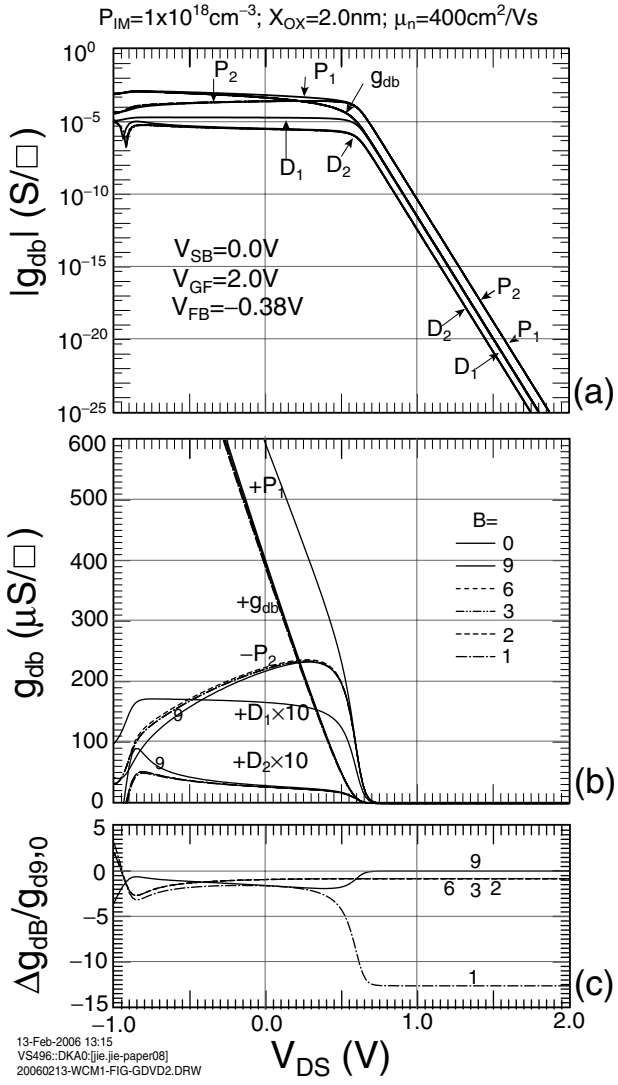

Figure 12: Drain or Output conductance versus drain voltage characteristics. (a) gd. Percentage deviation from gd9,0 (b) Semilog and (c) Linear

3.5 Body, Substrate or Source Bias Effects

The effects of body, substrate, or n++Source/p-Basewell bias are investigated. The drain current versus source/body voltage, V_{SB}, are presented in Fig.13 (a)-(d), which show that total currents I_{DB} and their percentage deviations all decrease with increasing reverse body bias. The drain current transfer characteristics, I_D versus V_{GF}, are presented in Fig.14(a)-(c). In the inversion range, the body bias causes nearly just a shift of the gate voltage axis by V_{SB}=+0.50V, as shown by the V_{SB}=0.0V curve in Fig. 14(a). However, the current in the accumulation range shown in Fig. 14(a) is substantially lowered by the 0.5V body bias, from 10^{-23} to 10^{-30} A/□.

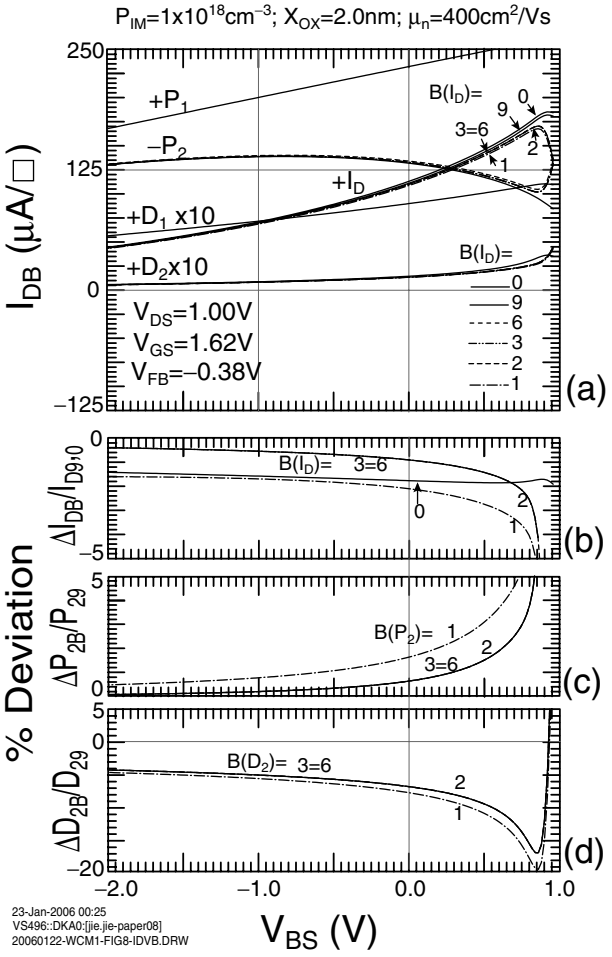

Figure 13 Effects of body bias on the drain current characteristics (a) I_{DB}. Percentage deviation of (b) total current $\Delta I_{DB}/I_{D9}$, (c) drift component $\Delta P_{2B}/P_{29}$ and (d) diffusion component $\Delta D_{2B}/D_{29}$.

4 SUMMARY

In this paper, the accuracies of the baseline long-wide channel model of the three commonly used compact models are evaluated. These compact models have used the surface-potential-based analytical approximation to the bulk-charge term, $Q_B \propto |U_S|^{1/2}$ (9604131), $|U_S-1|^{1/2}$ (9604132), and $|U_S-1+\exp(U_S)|^{1/2}$ (9604133). Our results show that they are adequate in the inversion range but poor in the subthreshold and accumulation range. An improved compact model (9604136) was tested which showed substantial improvement in the accumulation range, and gave adequate accuracy as baseline for advanced compact models. No discontinuity in conductance and trans-conductance was observed in these compact models.

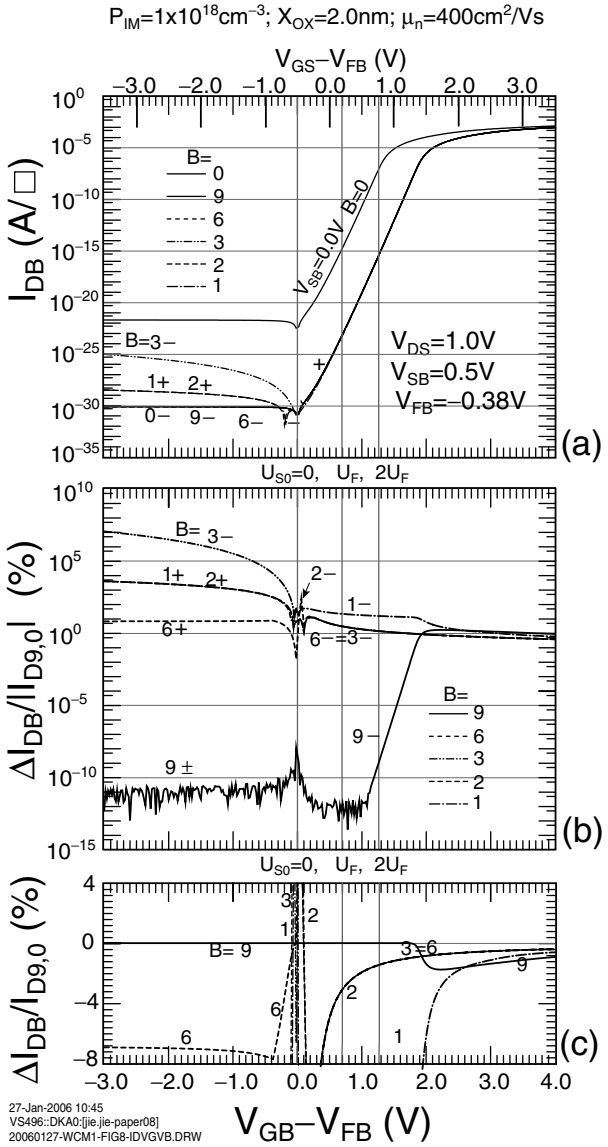

Figure 14 Effects of body bias on the transfer characteristics I_D-V_{GF}. B=1,2,3,6,9,0. (a) I_{DB}. Percentage deviation from $I_{D9,0}$ (b) Semilog and (c) Linear.

REFERENCES

[1] Chih-Tang Sah, "A history of MOS Transistor Compact Modeling," Keynote. Technical Proceedings Workshop on Compact Modeling (WCM), 349-390. Editors: Xing Zhou, Matthew Laudon and Bart Romanowicz. NSTI Nanotech 2005. The NSTI Nanotechnology Conference and Trade Show, May 8-12, 2005. Nano Science and Technology Institute, Cambridge, MA 02139, USA. #PCP05040394. **(2004-Sah)** On-line: http://www.nsti.org/publ/Nanotech2005WCM/1429.pdf

[2] Josef Watts, Colin McAndrew, Christian Enz, Carlos Galup-Montoro, Gennady Gildenblat, Chenming Hu, Ronald van Langevelde, Mitiko Miura-Mattausch, Rafael Rios, Chih-Tang Sah, "Advanced compact models for MOSFETs," ibd, 3-12. Online: http://www.nsti.org/publ/Nanotech2005WCM/1275.pdf

[3] Andrews C. Galup-Montoro, M. Schneider, V. C. Pahim and R. Rios, "Comparison of surface-potential-based and charge-based MOSFET core models," ibd, 13-18. http://www.nsti.org/publ/Nanotech2005WCM/1285.pdf

[4] Chih-Tang Sah, "Characteristics of the Metal-Oxide-Semiconductor Transistor," IEEE Trans. on Electron Devices,ED11(7),324-345,July1964.(**1964-Sah**)

[5] Chih-Tang Sah and Henry Pao, "The effects of fixed bulk charge on the characteristics of metal-oxide-semiconductor transistors," IEEE Trans. on Electron Devices, ED13(4),393-409, April 1966.(**1965-Sah-Pao**)

[6] Henry C. Pao and Chih-Tang Sah, "Effects of diffusion current on characteristics of metal-oxide (insulator)-semiconductor transistors," Solid-State Electronics, 9(10), 927-937, October, 1966. (**1966-Pao-Sah**)

[7] The first generations used the threshold-voltage model such as BSIM3. See: Yuhua Cheng, Min-Chie Jeng, Zhihong Liu, Jianhui Huang, Mansun Chan, Kai Chen, Ping Keung Ko, Chenming Hu, "A physical and scalable I-V model in BSIM3v3 for analog/digital circuit simulation," IEEE Trans. Electron Devices, vol. 44, No. 2, pp. 277-287, Feb., 1994 ; The latest upgrade BSIM-5 uses the inversion-charge model. See: Xuemei (Jane) Xi, Jin He, Mohan Dunga, Chiung-Hsun Lin, Babak Heydari, Hui Wan, Mansun Chan, Ali M. Niknejad, Chenming Hu, "The development of the next generation BSIM for sub-100nm mixed-signal circuit simulation," Tech. Proc. 2005-WCM, 233-236. Other BSIM articles can be found in http://www.device.eecs.berkeley.edu/~bsim3.

[8] G. Gildenblat, T. Chen, X. Gu, H. Wang, and X. Cai, "SP: An Advanced Surface-Potential-Based Model" Invited. 2003 IEEE International Conference on Electron Devices (IEDM) Technical Digest, 123-456, December 10, 2003.

[9] "Next Generation MOSFET model – May 25, 2005", Compact Model Council (affiliated with Electronic Industries Alliance) Press releases. Online: http://www.eigroup.org/CMC/press/ngmm_status_5_25.pdf.

[10] Gennady Gildenblat, et, al., E. van Langevelde, et. al. D. B. M. Klaassen, "Introduction to PSP MOSFET Model," Technical Proceedings Workshop on Compact Modeling (WCM), 19-24. Online: http://www.nsti.org/Nanotech2005/WCM2005/WCM2005-GGildenblat.pdf.

[11] M. Miura-Mattausch, D. Navarro, H. Ueno, H.J. Mattausch, K. Morikawa, S. Itoh, A. Kobayashi and H. Masuda, -"HiSIM: Accurate Charge Modeling Important for RF Era", Technical Proceedings of the 2003 Nanotechnology Conference and Trade Show, Volume 2, pp. 258 - 261. Online: http://www.nsti.org/Nanotech2003/WCM2003/WCM2003-MMiruaMattausch.pdf;
M. Miura-Mattausch, S. Hosokawa, D. Navarro, S. Matsumoto, H. Ueno, H.J. Mattausch, T. Ohguro, T. Iizuka, M. Taguchi, T. Kage, and S. Miyamoto, "Noise Modeling with HiSIM Based on Self-Consistent Surface-Potential Description", Technical Proceedings of the 2004 Nanotechnology Conference and Trade Show, Volume 2, pp. 66 - 69. Online: http://www.nsti.org/presentations/WCM2004/WCM2004-MMiuraMattausch.pdf.

[12] J. R. Brews, "A charge-sheet model of the MOSFET," Solid-state Electronics 21(2), 345-355, Feb. 1978. (**1978-Brews**)

[13] Bin B. Jie and Chih-Tang Sah, "Evaluation of surface-potential-based bulk-charge compact MOS transistor models," IEEE Trans. on Electron Devices, ED-52(8), 1787-1794, August 2005. (**2005-Jie-Sah**)

[14] Chih-Tang Sah, "Space charge theory of the MOS transistor," Version 11. Dec.12,1996, Unpublished. See [13] for a presentation of the original 1996-Sah rigorous derivation of the 4-component theory. (**1996-Sah**).

[15] Chih-Tang Sah, *Fundamentals of Solid-State Electronics – Study Guide,* 423pp, World Scientific Publishing Co., 1993. (**1993-Sah-FSSE-SG**)

MATHEMATICAL APPENDIX

This appendix gives the formulas to compute the transconductance and output conductance of the four components of the 9604139 model.

$$g_{mb}=g_{norm}\times(gm139P1+gm139P2+gm139D1+gm139D2) \quad (A1)$$
$$g_{db}=g_{norm}\times(gd139P1+gd139P2+gd139D1+gd139D2) \quad (A2)$$

It is straightforward to obtain the transconductance and output conductance of the two space-charge-limited components 9604139P1 and 9604139D1:

$$gm139P1=[(U_{GB}-U_{FB}-U_{SL})\times\partial U_{SL}/\partial U_{GB} - (U_{GB}-U_{FB}-U_{S0})\times\partial U_{S0}/\partial U_{GB}]/U_{II}^{1/2} \quad (A3)$$
$$gm139D1=(\partial U_{SL}/\partial U_{GB}-\partial U_{S0}/\partial U_{GB})/U_{II}^{1/2} \quad (A4)$$
$$gd139P1=(U_{GB}-U_{FB}-U_{SL})\times\partial U_{SL}/\partial U_{DB}/U_{II}^{1/2} \quad (A5)$$
$$gd139D1=\partial U_{SL}/\partial U_{DB}/U_{II}^{1/2} \quad (A6)$$

Because the bulk-charge drift depressment 139P2 is a double integral, it is not trivial to obtain the corresponding

transconductance. From (30), the following gm formula can be obtained:

$$gm139P2 = -\int_{U_{SB}}^{U_{DB}} \frac{\partial^2 U_S}{\partial U_{GB}\partial U_{NP}} \int_0^{U_S} \frac{\exp(U_P)[1-\exp(-U)]}{SignU_S \times F_X(U,U_N,U_P)} dU dU_{NP} \quad (A7)$$

$$-\int_{U_{SB}}^{U_{DB}} \frac{\exp(U_P)[1-\exp(-U_S)]}{SignU_S \times F_{SI}(U_S,U_N,U_P)} \frac{\partial U_S}{\partial U_{GB}}\bigg|_{U_{NP}} \frac{\partial U_S}{\partial U_{NP}}\bigg|_{U_{GB}} dU_{NP}$$

$$\frac{\partial^2 U_S}{\partial U_{GB}\partial U_{NP}} = \left(\frac{\partial U_S}{\partial U_{GB}}\right)^2 \times \left\{ \frac{\exp(U_S)-\exp(-U_S)}{F_{SI}(U_S,U_N,U_P)} signU_S\sqrt{U_{II}} \frac{\exp(-U_{NP})}{\sqrt{(P_{IM}/n_1)^2+4\exp(-U_{NP})}} - \right. \quad (A8)$$

$$\frac{\partial U_S}{\partial U_{NP}} \times \left[\frac{\exp(U_P)\times(1-\exp(-U_S))+\exp(-U_N)\times(\exp(U_S)-1)}{2\times F_{SI}(U_S,U_N,U_P)\times F_{SI}(U_S,U_N,U_P)} + \right.$$

$$\left. \left. signU_S\sqrt{U_{II}} \frac{\exp(U_P-U_S)-\exp(U_S-U_N)}{F_{SI}(U_S,U_N,U_P)} \right] \right\}$$

From section 3, it has been known that the drain current components 139P1 and 139P2 cancel each other in the accumulation, deep-subthreshold, and subthreshold ranges, because the total drift current is very small compared with the total diffusion current. Therefore, gm139P2 = −1 ×gm139P1 is valid for these three regions. Based on this, it is observed that (A8) works in these three regions. However, from the numerical slope of drain current 139P2, it was shown that A(8) deviates from the slope by one order of magnitude in the strong inversion range. Thus, other gm formulations or formulas are needed. From the original form of (30) as listed below

$$139P2 = -\int_{U_{S0}}^{U_{SL}} \int_0^{U_S} \frac{\exp(U_P)[1-\exp(-U)]}{SignU_S \times F_X(U,U_N,U_P)} dU dU_S \quad (A9)$$

the correct formula of gm139P2 can be derived and is

$$gm139P2 = -\frac{\partial U_{SL}}{\partial U_{GB}} \int_0^{U_{SL}} \frac{\exp(U_{PL})[1-\exp(-U)]}{SignU_{SL} \times F_X(U,U_{NL},U_{PL})} dU \quad (A10$$

$$+\frac{\partial U_{S0}}{\partial U_{GB}} \int_0^{U_{S0}} \frac{\exp(U_{P0})[1-\exp(-U)]}{SignU_{S0} \times F_X(U,U_{N0},U_{P0})} dU$$

$$-\int_{U_{SB}}^{U_{DB}} \int_0^{U_S} \frac{[1-\exp(-U)]}{SignU} \frac{d}{dU_{NP}} \left[\frac{\exp(U_P)}{F_{SI}(U,U_N,U_P)} \right] dU \times \frac{\partial U_{NP}}{\partial U_{GB}}\bigg|_{U_S} \frac{\partial U_S}{\partial U_{NP}}\bigg|_{U_{GB}} dU_{NP}$$

From (33), the gm139D2 formula is:

$$gm139D2 = \frac{\partial U_{SL}}{\partial U_{GB}} \times \frac{\exp(U_{PL})\times(1-\exp(-U_{SL}))}{signU_{SL}\times F_{SI}(U_{SL},U_{NL},U_{PL})} - \frac{\partial U_{S0}}{\partial U_{GB}} \times \frac{\exp(U_{P0})\times(1-\exp(-U_{S0}))}{signU_{S0}\times F_{SI}(U_{S0},U_{N0},U_{P0})} \quad (A11)$$

A transformation of (A11) is needed to remove the numerical noise in the accumulation, deep-subthreshold, and subthreshold ranges.

Similarly, the following g_d formulas are derived from (30) and (33):

$$gd139P2 = -\frac{\partial U_{SL}}{\partial U_{DB}} \int_0^{U_{SL}} \frac{\exp(U_{PL})\times(1-\exp(-U))}{SignU_{SL}\times F_{SI}(U_{SL},U_{NL},U_{PL})} dU \quad (A12)$$

$$gd139D2 = \frac{\partial U_{SL}}{\partial U_{DB}} \times \frac{\exp(U_{PL})\times(1-\exp(-U_{SL}))}{SignU_{SL}\times F_{SI}(U_{SL},U_{NL},U_{PL})} + \int_0^{U_{SL}} \frac{1-\exp(-U)}{SignU_{SL}} \times \frac{d}{dU_{DB}} \left[\frac{\exp(U_{PL})}{F_{SI}(U,U_{NL},U_{PL})} \right] dU \quad (A13)$$